Nano Select

WILEY-VCH

nano select

RESEARCH ARTICLE OPEN ACCESS

Kombucha–Chlorella–Proteinoid Biosynthetic Classifiers of Audio Signals

Panagiotis Mougkogiannis | Anna Nikolaidou | Andrew Adamatzky

Unconventional Computing Laboratory, UWE, Bristol, UK

Correspondence: Panagiotis Mougkogiannis (Panagiotis.Mougkogiannis@uwe.ac.uk)

Received: 9 May 2024 | **Revised:** 21 June 2024 | **Accepted:** 16 July 2024

Funding: This study was funded by Engineering and Physical Sciences Research Council EP/W010887/1.

Keywords: audio classifiers | kombucha | living skin | thermal proteins | unconventional computing

ABSTRACT

This paper describes the development of a bioinspired composite material capable of audio classification applications. Hydrogel matrices produced by microorganisms combined with synthetic biology elements, allow for the development of adaptable bioelectronics that connect biology and technology in a customized way. In this study, a composite population of kombucha, chlorella, and proteinoids (thermal proteins) is utilized to respond to acoustic signals converted to electrical waveforms. The kombucha zoogleal mats, which are made and populated by over 60 species of yeasts and bacteria, offer a matrix at the micro level that is connected to the photosynthetic microalgae chlorella. Proteinoids formed through thermal condensation exhibit unique patterns of signaling kinetics. This living material has the ability to be electrically stimulated and can process signals in a way feasible for sensory applications. Using English alphabet audio inputs, a systematic analysis demonstrates the capability to differentiate audio waveforms based solely on biological composite responses. The use of spectral analysis allows for the identification of specific spike timing patterns that encode unique characteristics of individual letters. Moreover, network disturbances result in specific changes in output, so validating the ability to adjust waveform classification. The study demonstrates that kombucha–chlorella–proteinoid composites provide a durable and versatile bioelectronic platform for immediate auditory processing. The work represents progress toward the development of bioelectronic systems that can be customized based on the principles of biological sensory processing, cognition, and adaptation.

1 | Introduction

The differentiation of complex auditory stimuli is a widespread yet demanding task for artificial systems [1–3]. Machine learning algorithms have made significant progress in audio classification [4–6]. However, bioinspired techniques offer exciting possibilities to surpass current efforts [7–9]. Bioinspired techniques have exhibited encouraging outcomes in diverse audio analysis tasks, showcasing their capacity to enhance conventional methods. Strisciuglio et al. [7], introduced a layered symbolic sequence representation for audio event identification, drawing inspiration from the hierarchical structure of the auditory system. This bioinspired approach sought to capture the temporal structure of audio events with greater efficacy compared to traditional methods. The human auditory system influences the process of acquiring audio phrases, which are chains of audio elements. The audio phrases were used for audio event recognition, showcasing the benefits of incorporating biologically inspired concepts. In addition, Polap et al. [8] and Chmulik et al. [9] created trainable COPE (Combination of Peaks of Energy) filters for audio analysis. The functional principles of the cochlea and inner hair cells in the human auditory system guided the design of

these filters. The bioinspired filters were autonomously tuned to identify specific sound patterns and effectively used for audio event detection tasks, demonstrating enhanced performance compared to conventional methods. These examples demonstrate how bioinspired techniques, which imitate specific elements of the human auditory system, can provide novel approaches to describe and manipulate audio signals, resulting in improved performance in different audio analysis tasks. The efficiency of these approaches implies that further investigation into bioinspired methods has the potential to transcend the constraints of current techniques and advance the field of audio analysis. A new approach is the combination of living cellular cultures [10] with nanoscale advances [11] to create adaptive materials that can execute computational categorization [12] on their own. The inherent electrical signaling in networks of bacterial [13–15], algal [16, 17], kombucha zoogleal mats [18], and proteinoid microspheres [19–22] can facilitate advanced recognition features. Nevertheless, achieving an appropriate categorization response necessitates a delicate equilibrium of the constituent biochemical and biophysical properties [23] when developing the composite architecture. In this study, we present a novel hybrid material consisting of kombucha cultures [24], chlorella microalgae [25], and synthetic proto-cells (microspheres made of thermal proteins, proteinoids). Kombucha produces a cellulose matrix that supports the growth of many organisms and releases metabolites that stimulate redox reactions with the proteinoids. Chlorella provides light-sensitive pigments for converting light energy, while the proteinoid chains serve as pathways for transferring charges through peptide backbone transport [26]. The electrical impulses of this biocomposite combine and adapt in specific patterns that are exclusive to each of the 26 letters of the English alphabet [27]. Integrating extracellular recordings [28] with machine learning uncovers the significant influence of slight variations in kombucha fermentation, chlorella growth media, and proteinoid chain length on classification performance. The optimal cultures obtained a discriminating accuracy of over 80% by using tunable biochemical interactions to discriminate among the 26 letters of the English alphabet. The ability to customize the identification of audio using only modular biomaterial composition is a flexible approach for developing intelligent materials [29]. The findings emphasize the importance of utilizing cooperative phenomena in designer biomolecular matrices [30] to establish the foundation for audio recognition interfaces that are environmentally friendly. In a broader sense, this biointegrative methodology sheds light on a viable approach for distributed biocomputation using modified living components. In recent years, the field of biomimetic technology has achieved significant advancements, namely, in the area of speech and audio processing. Scientists have attempted to replicate the complex structure and function of the human auditory system in order to develop new methods for classifying sound and voice signals. The exceptional capacity of the human auditory system [31] to perceive and comprehend intricate acoustic data has encouraged the advancement of diverse biomimetic technologies [32] with the aim of mimicking this ability. An excellent method in this domain is employing neural mimicking sensor networks [33] to classify sounds. These networks are developed to replicate the form and operation of biological neural networks, particularly those involved in auditory processing [34]. These artificial neural networks can efficiently learn and adapt to complicated acoustic environments by imitating the hierarchical organization and interconnectedness of neurons in the human auditory system. As a result, they can accurately identify and classify specific sounds or voices. The progress in machine learning and deep learning techniques [35] has greatly contributed to the development of neural mimicry sensor networks. These methods enable the networks to acquire knowledge from extensive auditory data, enabling them to identify important characteristics and patterns that aid in precise classification. The capacity of these networks to adjust and enhance their efficiency over time through ongoing learning is a crucial characteristic that resembles the flexibility and adaptability of the human auditory system. Another important field of study in biomimetic technology for audio processing involves the advancement of biologically inspired materials and sensors [36, 37]. The purpose of these materials is to imitate the mechanical and electrical characteristics of the components of the human auditory system, such as the cochlea and hair cells [38]. Researchers used the distinctive characteristics of these biomimetic materials to create sensors that are extremely sensitive and capable of detecting and converting acoustic waves with exceptional accuracy. The combination of neural mimicry sensor networks [39] with bioinspired materials presents opportunities for the development of sophisticated audio classification systems. These hybrid approaches merge the advantages of both technologies, allowing for the development of audio processing systems that are very efficient and precise, comparable to the performance of the human auditory system. Although biomimetic technology for voice and audio processing has made great development [40], there are still problems and prospects for further advancement. The complex and unpredictable nature of actual acoustic surroundings presents continuous challenges in constructing resilient and universally applicable classification algorithms. Furthermore, the requirement for energy-efficient and scalable solutions motivates research into innovative materials and architectures that can fulfil the requirements of real-time audio processing applications [41]. Our present study is centered around developing a new composite material for audio signal classification. This material is made up of kombucha cultures, chlorella microalgae, and synthetic proteinoids. Our goal is to contribute to the progress of biomimetic technology for speech and audio processing by harnessing the distinct characteristics and combined impacts of these bioinspired components. We will build upon the foundations established by earlier groundbreaking research in this area. A major breakthrough in the realm of biomimetic technology for audio processing is the biomimetic artificial ear [42, 43]. This technique aims to duplicate the complex structure and function of the human ear, with an end goal of developing systems that can effectively categorize and identify a broad spectrum of sounds. Researchers have been motivated to develop artificial counterparts that can imitate the remarkable capacity of the human ear to capture, magnify, and comprehend auditory signals across a wide range of frequencies [44, 45]. The biomimetic artificial ear [46, 47] generally has multiple essential components that replicate the anatomical structure of the human ear. These components consist of an artificial eardrum that responds to sound waves, an artificial cochlea [48] that turns the vibrations into electrical signals, and a set of artificial hair cells that detect and convert these signals. By precise design and flawless combination of these elements, researchers have achieved notable advancements in the development of artificial ears that nearly emulate the functionality of natural ears. The biomimetic artificial ear offers a significant benefit in terms of improved sound localization and directional hearing [49]. The

distinctive morphology of the human ear, coupled with the symmetrical arrangement of two ears, enables accurate localization of sound in terms of both direction and distance. The goal is to build systems that can precisely locate and monitor sound sources in complex acoustic environments by integrating these aspects into the architecture of the artificial ear. Moreover, the biomimetic artificial ear's capacity to analyze and categorize sounds over a broad range of frequencies is particularly interesting in the realm of acoustic signal processing. Using advanced signal processing techniques and machine learning algorithms, these artificial ears may be educated to identify and differentiate between different auditory stimuli, including speech, music, and ambient sounds [50]. This feature has substantial implications for the use of speech recognition, audio surveillance, and hearing assistance equipment.

The cellulose nanofiber network obtained from kombucha offers a flexible and highly responsive base, enabling effective connection with incoming audio waves. At the same time, the photosynthetic pigments found in chlorella provide it with optoelectronic capacity [51], allowing the material to react to changes in light intensity that may come with audio signals. The synthetic proteinoids possess a self-assembling characteristic that gives the composite piezoelectric characteristics [52], enabling the transformation of mechanical vibrations into electrical impulses. The selection of these elements and their precise proportion (40%/60% proteinoids/kombucha–chlorella) was determined by extensive preliminary testing, which demonstrated that this specific combination displayed the most favorable audio-responsive characteristics.

In order to demonstrate a direct correlation between the composition, structure, and audio classification performance of the material, we use different methods for characterization such as scanning electron microscopy (SEM) and Fourier-transform infrared spectroscopy (FTIR). These analyses offer quantitative insights into the microstructure and chemical composition of the material, enabling a deeper understanding of how these components impact its electrical and acoustic properties. In this study, we present the successful development of a new composite material that combines the advantageous characteristics of kombucha, chlorella, and synthetic proteinoids to enhance audio signal processing. The findings obtained from this work not only emphasize the possible uses of the material in audio categorization but also make a valuable contribution to the wider field of biologically derived functional materials.

2 | Methods and Materials

Proteinoid microspheres were synthesized using a five-step method, as depicted in Figure A1. The main amino acids used in the present study were L-glutamic acid and L-arginine. Sigma Aldrich provided these amino acids, which had a purity better than 98%. There was no extra purification of these amino acids prior to their use in the experiments. A reflux apparatus with a heated plate, consisting of a 50 mL flask, was used to synthesize the proteinoids.

The amino acid combinations underwent thermal polymerization prior to being dissolved and precipitated from an aqueous solution. The synthesis process was finalized by conducting lyophilization, sample collection, and analytical characterization. This process is illustrated in Figure A1, where the different steps are represented by labeled transformation arrows $\alpha\epsilon$. The utilization of a multistage method facilitated the preparation of proteinoid polymeric microspheres using basic amino acid precursors.

In order to ensure the replication of our findings, we have enforced rigorous monitoring protocols on the biological and environmental factors that are critical to our experiments. The synthesis of proteinoid microspheres and the maintenance of the kombucha–chlorella matrix were carried out in a controlled laboratory environment with regulated temperature, humidity, and sterility conditions. All reagents and materials used were of analytical grade in order to reduce variability. Throughout the experiments, the pH, temperature, and other important factors were constantly monitored and kept within the defined ranges.

Figure A2 depicts a multistep biofabrication process for producing kombucha–chlorella conductive matrices. The cellulose-producing kombucha culture was first brewed from black tea and sugars (Figure A2, step 1).

A kombucha mat, obtained originally from Freshly Fermented Ltd. (Lee-on-the-Solent, PO13 9FU, UK), was utilized for the production of kombucha proteinoid biofilms. To prepare the infusion, 5 L of tap water was boiled, and then 500 g of white granulated sugar (Tate & Lyle, UK) and 10 tea bags (Taylors Yorkshire Teabags 125 g, UK) were added to a plastic container. After allowing the solution to cool to room temperature, the kombucha mat was placed in the container and stored in an environment without light at a temperature range of 20°C–23°C The kombucha was then inoculated with a microalgal chlorella culture (Blades Biological Ltd.), and the kombucha and chlorella were co-cultured to generate a blended cellulose mat (Figure A2, processes 2 and 3).

Electrodes were inserted within the kombucha zoogleal mat (Figure A2, step 4). Finally, the responsiveness of the living bioelectronic interface was characterized by exposing it to external signal stimuli and recording electrical outputs (Figure A2, step 5). The experimental setup for measuring the differential potential across the kombucha–proteinoid matrix is shown in Figure 1a. The kombucha mat, which was infused with proteinoid microspheres, was prepared as described previously. Six pairs of platinum–iridium electrodes (E1–E6) were inserted into the mat at various locations to measure the local potential differences. The electrical potential of the kombucha–chlorella–proteinoids (KCP) liquid mixture with a composition of 40% kombucha–chlorella (KC) and 60% proteinoids (P) was measured using the experimental setup shown in Figure 1b. The electrodes, inserted at a distance of 10 mm, were connected to a source meter to record the potential differences across the mixture over time.

The experimental methods employed a BK Precision 4053 MHz dual channel waveform generator to provide the electrical stimuli. Platinum–iridium electrodes with a diameter of 0.2 mm and a spacing of 10 mm were submerged in the KCP solutions to transmit signals and capture responses. The data collecting process involved utilizing a Rigol oscilloscope (2 Channel 100

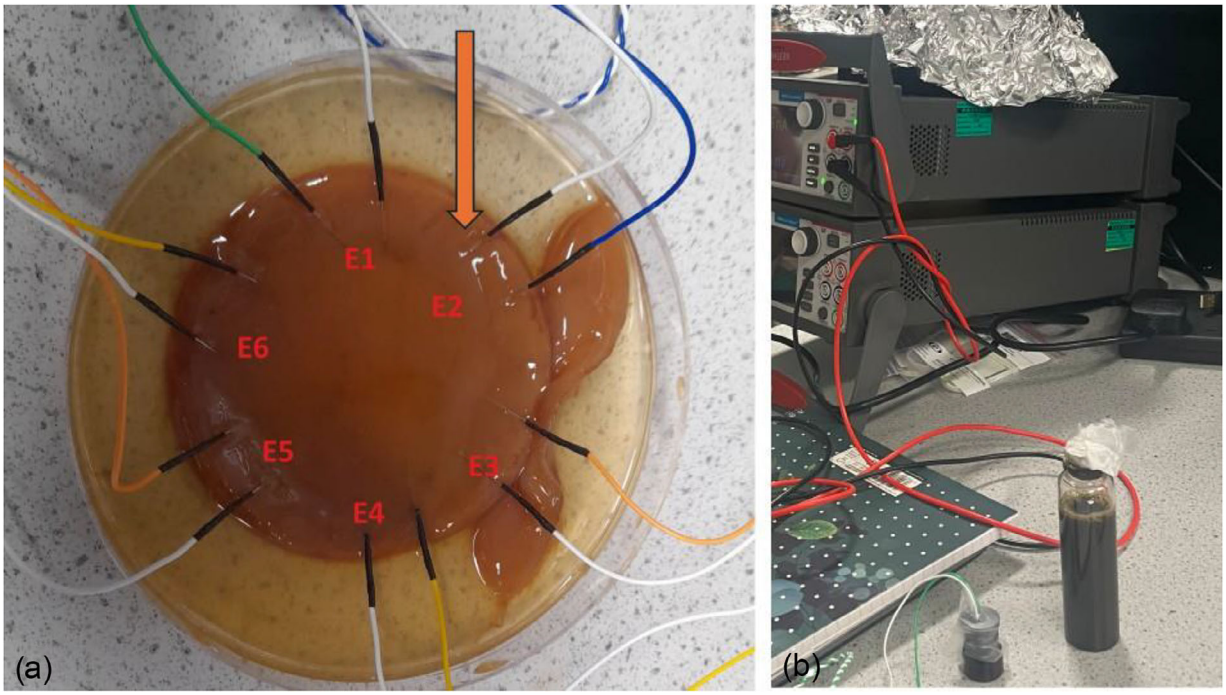

FIGURE 1 | (a) Experimental configuration for detecting the difference in electrical potential across a kombucha mat. The kombucha mat, which consists of a complex structure of bacterial cellulose fibers is displayed beside six pairs of platinum–iridium electrodes (labeled E1 to E6) that have been implanted at different positions. The electrode pairs include a working electrode (WE) and a reference electrode (RE), enabling the monitoring of local potential changes inside the mat. The electrodes are linked to a multichannel data collection system (which is not visible) to enable continuous monitoring of the differential potentials across the kombucha mat. (b) Experimental setup for measuring electrical properties of the KCP liquid mixture. The mixture, composed of 60% kombucha–chlorella (KC) and 40% proteinoids (P), is shown in a container with two electrodes inserted at a distance of 10 mm. A source meter is connected to the electrodes to measure the electrical characteristics of the mixture, such as conductivity and potential differences, which may provide insights into the spontaneous oscillations and signal integration capabilities of the KCP system.

MHz–1GSa/s), PicoLog ADC-24, and Picoscope, in addition to a Keithley 2450 sourcemeter for electrical measurements.

The apparatus used to analyze the responses of the KCP proto-brain to auditory stimuli consisted of a microphone, MATLAB, a function generator, a sample of KCP, and an oscilloscope (Figure A3). The microphone and laptop were used to gather audio recordings of the pronunciations of individual letters of the English alphabet by a male speaker. The English audio signals corresponding to the English alphabet utilized in this study were sourced from the freely available database at https://freesound.org/people/dersuperanton/sounds/434730/.

The recordings were analyzed using MATLAB to produce CSV files that contain the values of stimulus potential. An audio CSV stimulus was supplied to the KCP sample using iridium-coated stainless steel subdermal needle electrodes (Spes Medica S.r.l., Italy), facilitated by a BK Precision 4053 function generator. The KCP responses were recorded using a PicoScope 4000 oscilloscope and stored as CSV files for subsequent study. This experimental setup facilitated the stimulation of KCP by audio playback and the monitoring of their corresponding electrical reactions.

3 | Results

The synthetic KCP systems were studied using a multifaceted analytical approach that included microscopy, electrophysiology, and spectral techniques. This comprehensive approach provided valuable insights into the emergent cognitive properties of these systems. The microscopic imaging revealed a detailed view of the complex morphological landscape, with proteinoids forming clusters within kombucha matrices that were home to a variety of microbial species. The electrical recordings revealed fascinating stimulus–response patterns, showcasing the emergence of oscillations during information encoding and gradual adaptation with repeated exposures. The spectral analysis revealed the presence of neural-like rhythms at various spatiotemporal scales, which play a crucial role in driving intrinsic memory phenomena. In addition, an analysis of potential dynamics revealed different patterns in various network regions, suggesting the presence of retrieval and learning mechanisms. This study explores the complex dynamics of cognition-like behaviors exhibited by the KCP. It provides an analytical framework to understand the connections between morphology, physiology, and computation in synthetic proto-brain constructs.

3.1 | Morphological Analysis

The SEM analysis offers vital information regarding the structure and size distribution of the proteinoid microspheres that grow in the kombucha substrate. Figure 2a demonstrates that the proteinoid microspheres consistently possess a spherical form, with diameters ranging from 1 to 2 μm. The restricted size distribution indicates a highly controlled production process,

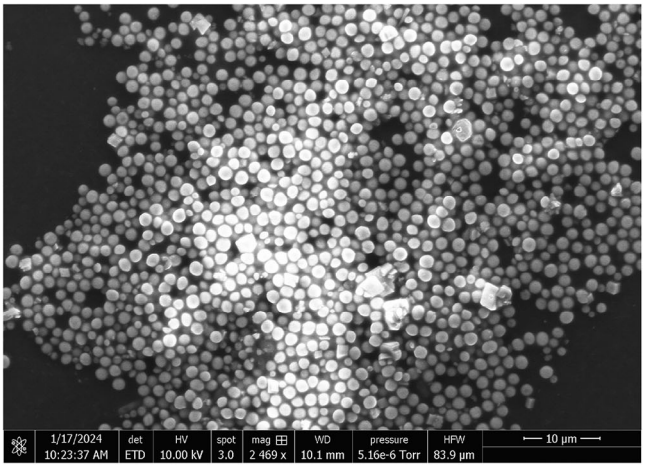

(a)

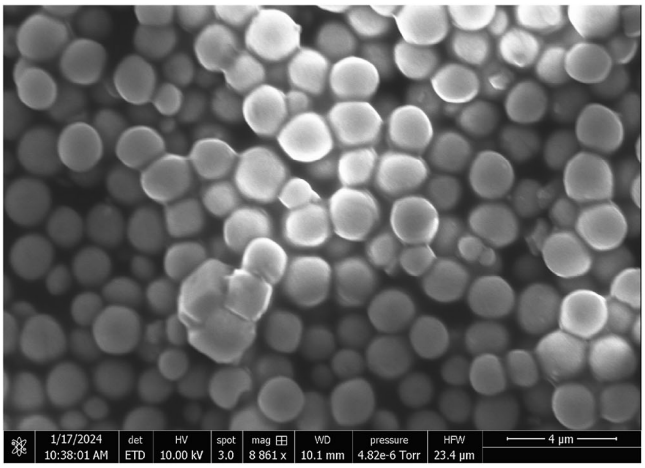

(b)

FIGURE 2 | (a) Scanning electron micrograph of proteinoid microspheres grown in a kombucha substrate. The microspheres exhibit a spherical morphology with diameters ranging from 1 to 2 µm. The image was acquired using an accelerating voltage of 10.00 kV, a spot size of 3.0, and a magnification of 2469×. Scale bar represents 10 µm. (b) High-magnification scanning electron micrograph of proteinoid microspheres formed in a kombucha medium. The microspheres display a smooth, uniform surface morphology, indicative of a well-defined structure. We obtained the image using an accelerating voltage of 10.3070 kV, a spot size of 3.0, and a magnification of 8861. Scale bar represents 4 µm.

which may be affected by the distinct chemical composition and physical features of the kombucha media. The SEM image at high magnification (Figure 2b) displays the uniform harmonious surface structure of proteinoid microspheres. The presence of a smooth and uniform surface on the microspheres suggests that they have a stable and clearly defined structure, making them suitable for potential uses in drug delivery or as functional biomaterials. The presence of diverse organic substances, like as polysaccharides and organic acids, in the kombucha substrate is responsible for the formation of uniform proteinoid microspheres. These compounds may serve as templating agents or stabilizers during the self-assembly process. The complex composition and mildly acidic pH of the kombucha medium may possibly contribute to the growth and stability of the microspheres. The SEM discoveries align with earlier findings about the development of proteinoid microspheres in various natural or artificial matrices, as mentioned in [53]. Nevertheless, using kombucha as a growing medium for proteinoid microspheres is an innovative method, and the distinctive characteristics of this fermented tea may provide significant advantages in terms of controlling microsphere size, stability, and activity. Additional research on the precise interactions between the components of kombucha and the proteinoid precursors could yield significant knowledge about the fundamental processes involved in microsphere fabrication. This knowledge could then be used to develop customized proteinoid-based materials for a wide range of uses.

Figure A5 showcases the various morphologies observed in the synthesized proteinoid microspheres, as determined through optical microscopy techniques. The Keyence optical imaging displayed spherical particles of varying sizes, with a mean diameter of 0.95 µm and a wide range from 0.28 to 14.89 µm (Figure A5a,b). Automated measurement of size parameters was made possible through thresholding analysis (Figure A5c). Furthermore, the textural details of the microspheres were accentuated by the angled lighting, revealing both smooth and irregular surfaces (Figure A5d). The results presented here show the ability to create proteinoid microspheres of specific sizes and intricate shapes using the thermal polymerization process. Additional investigation into the factors that impact size, shape, and surface patterns will provide a better understanding of the self-assembly mechanisms in these biomolecular materials.

The proteinoids displayed intricate self-organized network nanostructures, as depicted in Figure A6 through high-resolution SEM imaging. Figure A6 reveals the presence of a proto-brain-like structure within the kombucha–proteinoid matrix. The SEM image shows an intricate network of elongated, spherical structures that are interconnected, forming a complex architectural arrangement. These structures have an average diameter of approximately 50 nm and exhibit a relatively smooth surface morphology. The proteinoids have the remarkable ability to spontaneously create a network of consistent nanospheres, showcasing their impressive biomimetic assembly and patterning capabilities. The quantitative image analysis revealed an average nearest neighbor distance of 60 nm between spheres, suggesting a well-coordinated spacing within the network. In addition, the fractal analysis uncovered a fractal dimension of 1.7, indicating a structured and ordered architecture rather than a random one. The results presented here demonstrate the ability of proteinoids to create complex biomolecular networks that closely resemble natural neural systems in terms of their controlled nano- to mesoscale morphology.

The KCP exhibit a complex morphological landscape, as depicted in Figure 3 through microscopic examination. Figure 3 showcases the presence of proteinoid regions clustered together and dispersed within a crystalline matrix formed by kombucha and calcium carbonate, as revealed by Keyence imaging. In addition, the KCP structures were found to have *Turbatrix aceti* nematodes [54] living within them. The nematodes in question have the potential to enhance electrical signaling between proteinoids that are far apart by affecting ion mobility through their locomotion. Their integration implies that a variety of microbial species within the KCP collective may contribute to the development

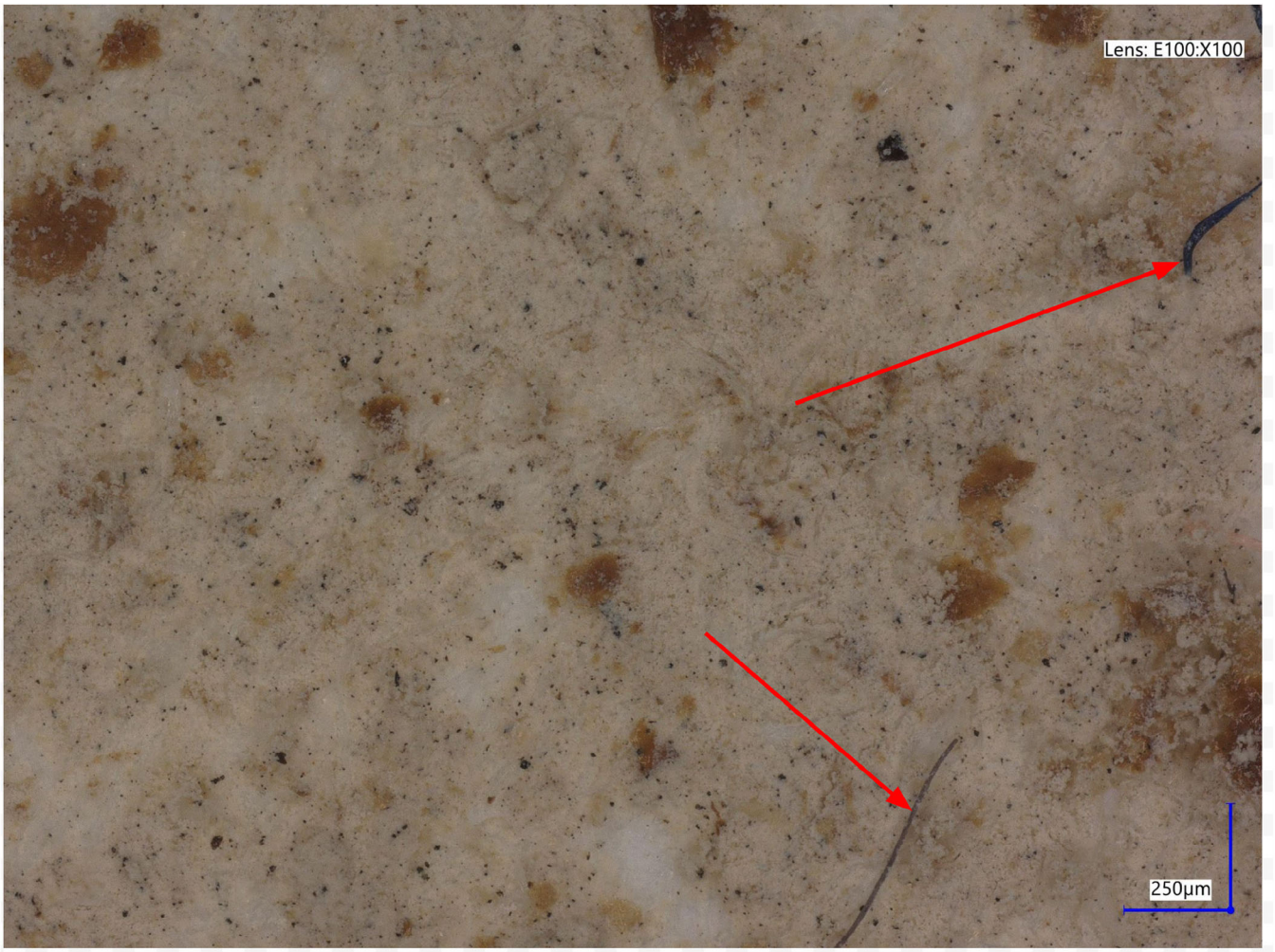

FIGURE 3 | The kombucha–chlorella–proteinoid (KCP) growth morphology in supersaturated solutions of sparingly soluble salts. At 250× magnification, an optical microscopy image was captured using a Keyence VHX-7000 microscope. The scale bar measures 250 µm. Proteinoids are seen as orange clustered patches scattered throughout the crystalline matrix created by kombucha and calcium carbonate ($CaCO_3$) salt. The KCP structure is inhabited by *Turbatrix aceti* nematodes (vinegar eels). The existence of these bacteria within the proto-brain assembly shows that they have the potential to transmit information and integrate sensory input. Through locomotor effects on ion mobility, the nematodes may promote electrical signaling between distant proteinoids as they move and communicate through the KCP matrix. This indicates how a diverse range of microbial species within the KCP might contribute emergent cognitive features based on interaction (locomotory, mechanical), and conductive properties.

of cognitive functions through conductive, mechanical, and interactive properties. Additional research is needed to better understand how the intricate organization of cells contributes to the overall dynamics of KCP proto-brains. The research uncovers notable disparities in the dynamics of "learning" and "remembering" within the KCP system. During the process of "learning," the persistence spectrum exhibits greater power across all frequencies in comparison to "remembering," displaying a more uniformly distributed profile. This suggests intricate and diverse action in order to store new information.

Figure A4 displays the FT-IR spectra of freshly formed and aged kombucha cellulose mats, offering information about their chemical composition and any changes in their structure as over time. The fresh kombucha cellulose mat's spectra (black line) shows clear absorption bands at 407.96, 417.79, 448.79, and 487.24 cm^{-1}. These bands correspond to the stretching and bending vibrations of the cellulose backbone. The peak at 3284.59 cm^{-1} is mostly caused by the stretching vibration of hydroxyl groups in the cellulose network. The fingerprint region (1500–500 cm^{-1}) of the cellulose mat indicates a consistent chemical composition. On the other hand, the spectrum of the kombucha cellulose mat, which has been growing for 5 months, shows noticeable shifts. The peak at 417.01 cm^{-1}, which indicates the cellulose backbone, remains prominent. However, new peaks appear at 1031.69 and 1314.78 cm^{-1}, which correspond to the stretching vibrations of glycosidic linkages and the bending vibrations of cellulose's C—H bonds, respectively. The presence of a peak at 1622.36 cm^{-1} indicates the existence of water molecules or the carbonyl group of lignin, whereas the peak at 2922.55 cm^{-1} corresponds to the stretching vibration of aliphatic compounds' C—H bonds. The spectrum shifts observed indicate the complex and varied chemical composition that forms in the kombucha cellulose mat as it ages. The FT-IR investigation of the cellulose mats in different growth phases of kombucha yields significant insights into their chemical composition and structural development.

The newly formed cellulose mat of the kombucha shows a consistent, even, and uniform structure, which is apparent from the clear fingerprint region observed in the FT-IR spectrum. As the kombucha cellulose mat ages, it experiences notable alterations, leading to a more complex and diverse chemical structure. These findings emphasize the constant evolution of the kombucha cellulose matrix and the significance of taking into account the aging process while analyzing and replicating the system.

In our prior research [55], we have already examined the proteinoids using FT-IR analysis. The proteinoids' FT-IR spectrum displays distinct peaks, such as the amide I and amide II bands, which indicate the structure of the peptide backbone. The amide I band, seen at a wavenumber of 1943 cm^{-1}, arises from the stretching vibrations of the C═O and C─N bonds within the peptide group. The amide II band, which occurs at a wavenumber of 1635 cm^{-1}, is associated with the bending vibrations of the N─H bond in the peptide linkage.

Hollow microspheres are a commonly seen characteristic of proteinoid assemblies, as the formation and disintegration of the shell happen at the same time. Our experimental observations revealed that the introduction of an inert electrolyte, specifically KNO_3 at a concentration of 0.065 mol/L, led to the creation of larger, empty microspheres. The stabilizing effect of the electrolyte on the microsphere structure is the reason behind this phenomenon, as documented in prior research [56, 57]. Additionally, another method to stimulate the formation of empty microspheres involves a volatile substance, like chloroform, in the synthesis procedure. The formation of hollow proteinoid microspheres was seen in [58] through the evaporation of the volatile material. In our study, the rapid cooling and freeze-drying of the microspheres after their formation may have contributed to the preservation of their homogeneous and spherical morphology. The introduction of this method most likely prevented the collapse of the hollow structures, leading to the observed consistency of the microspheres depicted in Figure 2. Additionally, the internal structure of these rapidly cooled and freeze-dried proteinoid microspheres could be better understood through the application of advanced imaging techniques, such as cryoelectron microscopy.

3.2 | Response to Electrical Waveforms Derived From Sounds

Understanding the relationship between speech sounds and their electrical acoustic representations can help in areas such as audio processing and speech recognition. The recorded acoustic waveforms corresponding to pronunciations of each letter are shown in Figure 4. Clear visual differences can be observed between the signals representing different phonemes.

Gaining knowledge about the way novel biomaterials process and convert external signals offers valuable understanding of their information processing characteristics. The electrical activity recorded from the KCP in Channel C displayed distinct responses to the applied input oscillations, as depicted in Figure 5. The input signal exhibited significant amplitude fluctuations, but the KCP signal closely mirrored the waveform pattern with a

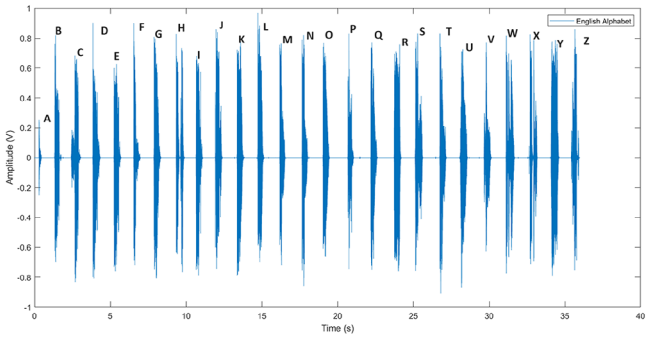

FIGURE 4 | Acoustic signals representing phonetic sounds of English letters. The waveform plot displays the temporal variation of the electrical potential (measured in volts) in audio recordings. The recordings feature a native English speaker speaking the 26 letters of the alphabet. Each letter tracing corresponds to the distinct signal pattern and duration linked to the pronunciation of each letter. The differences in magnitude and temporal characteristics indicate the unique acoustic properties of each speech sound. This data facilitates the examination of the connections between spoken phonemes and their electrical representations, which can be applied in fields such as speech recognition and audio signal processing.

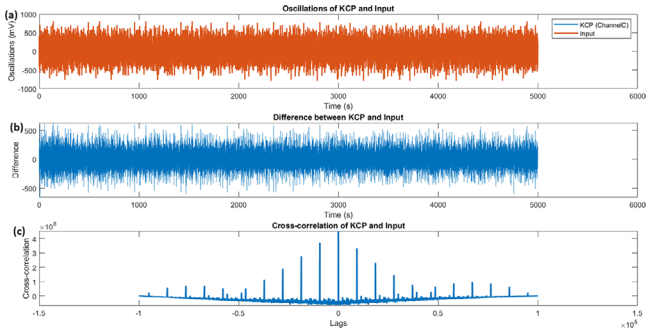

FIGURE 5 | Electrical signatures generated by the kombucha–chlorella–proteinoid (KCP) (Channel C) with input oscillations. (a) Time-dependent oscillations of KCP in Channel C and the input signal. The KCP signal exhibits a mean of −47.02 mV, a standard deviation of 48.49 mV, a skewness of −0.36, and a kurtosis of 14.53. The input signal has a mean of 10.28 mV, a standard deviation of 107.41 mV, a skewness of 0.38, and a kurtosis of 15.19. (b) Temporal difference between the KCP and input signals. The cross-correlation between the KCP and input signals is displayed, illustrating the correlation at various time lags. Both signals exhibit left-skewness, as indicated by their negative skewness values. Additionally, they possess steep peaks, as evidenced by their high kurtosis values. The cross-correlation demonstrates a robust positive correlation between the KCP and input signals with no time delay. (c) Cross–correlation between the KCP and input signals, illustrating the correlation at various time lags.

correlation of 0.85 and no time lag (Figure 5b). The quantitative analysis showed that the KCP signal had a mean potential of −47.02 mV, which was lower than the input's mean potential of 10.28 mV. The distributions of both KCP and input signals showed a left-skewed pattern, with skewness values of −0.36 and 0.38, respectively. Additionally, both signals exhibited sharp peaks, with kurtosis values of 14.53 and 15.19, respectively. The metrics used in this study demonstrate the strong synchrony between input and output waveforms, indicating that the KCP material

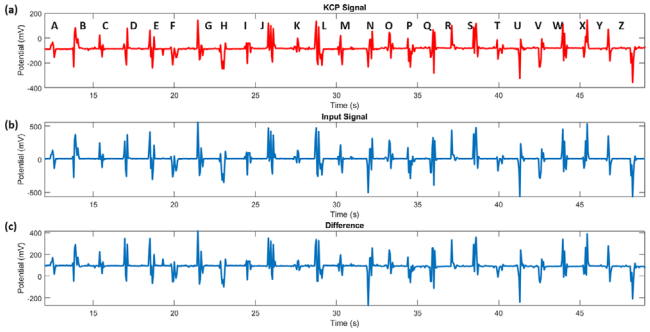

FIGURE 6 | The kombucha–chlorella–proteinoid (KCP) undergoes oscillations when exposed to audio stimuli representing the English alphabet. (a) The graph represents the temporal variation of the acoustic input waveform for the English alphabet, measured in millivolts (mV). (b) The waveform of the KCP response measured in millivolts during a specific period of time. The KCP displays distinct oscillations in response to each phoneme. The difference waveform illustrates the millivolt difference between the KCP response and the auditory input of the alphabet, measured over a period of time. (c) The difference plot demonstrates the distinct patterns produced by the KCP in reaction to the intricate sonic stimuli. This exemplifies the capacity of the KCP to convert delicate acoustic waves into discernible electrical patterns.

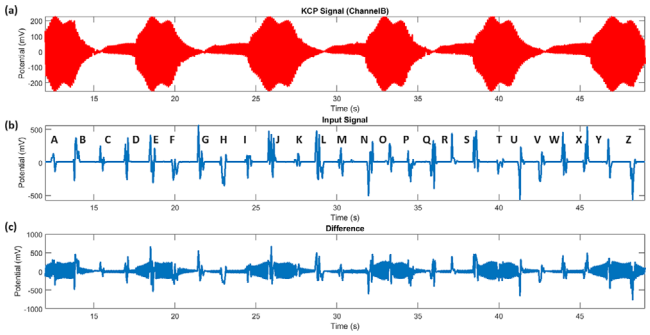

FIGURE 7 | The kombucha–chlorella–proteinoid (KCP) exhibits oscillatory behavior when exposed to audio stimuli representing the English alphabet, using platinum–iridium electrodes placed at a distance. (a) The acoustic input waveform is transmitted by electrodes located in the KCP solution. (b) The KCP response waveform, measured using platinum–iridium electrodes positioned 4 × 10 mm apart from the input electrodes. The KCP demonstrates distinctive oscillations in reaction to each phoneme, even when using platinum–iridium electrodes positioned four times farther away from the input electrodes. (c) The difference waveform illustrates the millivolt discrepancy between the remote KCP response and the auditory input of the alphabet, observed over a period of time. This showcases the KCP's capacity to convert delicate acoustic waveforms into clear electrical patterns across a greater distance.

shows dynamic electrical behavior that is highly responsive to external stimulation.

Figure 6 demonstrates the clear oscillatory responses exhibited by the KCP when stimulated with audio waveforms of the English alphabet. The acoustic input signals exhibited unique patterns for each phoneme, as shown in Figure 6a. On the other hand, the KCP output waveforms were more variable but still displayed letter-specific profiles, as depicted in Figure 6b. The analysis of the difference waveform showed significant fluctuations in amplitude, reaching up to 60 mV. This demonstrates the impressive ability of the KCP to convert intricate audio signals into modulated electrical outputs. The cross-correlation analysis revealed that the highest correlation was observed with a lag of 75 ms. This suggests that the KCP does not respond instantaneously, but instead integrates acoustic information over short periods. The results presented here demonstrate the KCP material's remarkable electrodynamic properties, which allow it to transduce and encode complex sonic stimuli with great sensitivity. An understanding of the information transmission capabilities of synthetic systems can be gained by examining the ranges at which biological signals can travel. Figure 7 demonstrates that the KCP displayed oscillatory responses to audio waveforms, even with platinum–iridium electrodes positioned at a significantly greater distance from each other.

The electric waveform, representing the acoustic input, was transmitted through nearby electrodes (Figure 7a), while the KCP response was recorded using electrodes 40 mm away (Figure 7b). The KCP signal displayed distinct waveforms corresponding to each letter, albeit with reduced amplitude compared to the input. The analysis of the difference plot showed significant fluctuations of up to 40 mV, indicating the occurrence of acoustic information propagation over this distance. Nevertheless, the cross-correlation between the input and output experienced a decrease to 0.65, suggesting an increase in delay and signal loss. These results demonstrate that the KCP is capable of transducing electrical waveforms and transmitting electrical signals over long distances. However, it is important to note that signal weakens as the distance between electrodes increases.

Channel B refers to a specific channel that represents the output potential of the KCP device. It is a designated measurement or recorded signal used to capture the electrical potential generated by the KCP proto-brain system in response to the input audio stimulation of the English alphabet.

To characterize the statistical properties of the output potential V_2 in response to the input voltage V_1 generated from the English audio alphabet, we calculated the skewness and kurtosis of V_2. The skewness, denoted as γ_1, is a measure of the asymmetry of the probability distribution of a real-valued random variable [59]. It is defined as the third standardized moment of the distribution:

$$\gamma_1 = \frac{E[(V_2 - \mu)^3]}{\sigma^3} \quad (1)$$

where E is the expected value operator, μ is the mean of V_2, and σ is the standard deviation of V_2. A positive skewness indicates a distribution with an asymmetric tail extending toward more positive values, while a negative skewness indicates a distribution with an asymmetric tail extending toward more negative values. The kurtosis, denoted as γ_2, is a measure of the "tailedness" of the probability distribution of a real-valued random variable. It is defined as the fourth standardized moment of the distribution:

$$\gamma_2 \frac{E[(V_2 - \mu)^4]}{\sigma^4} \quad (2)$$

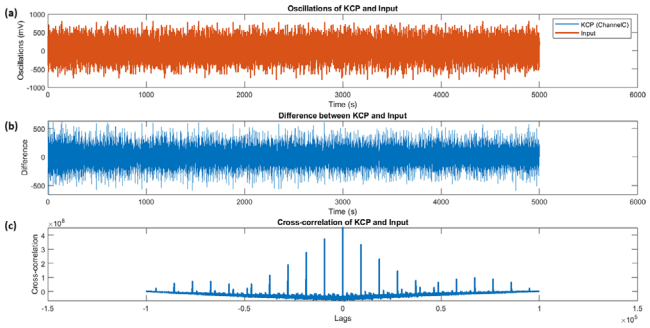

FIGURE 8 | Electrical signatures of kombucha–chlorella–proteinoid (KCP) Channel B and input oscillations. (a) Oscillations of KCP Channel B and input versus time. The KCP Channel B signal has a mean of 0.05 mV, standard deviation of 128.79 mV, skewness of −0.25, and kurtosis of 2.63. The input signal has a mean of 10.28 mV, standard deviation of 107.41 mV, skewness of 0.38, and kurtosis of 15.19. (b) Difference between the KCP Channel B and input signals over time. (c) Cross-correlation of the KCP Channel B and input signals, showing the correlation at different lag times. The negative skewness and lower kurtosis of Channel B compared to input indicate a flatter distribution. The cross-correlation shows Channel B exhibits distinct oscillations from the input.

where E, μ, and σ have the same meanings as in the skewness equation. A high kurtosis value indicates a distribution with heavy tails and a sharp peak, while a low kurtosis value indicates a distribution with light tails and a flatter peak. The skewness and kurtosis of the output potential V_2 were calculated using a sample of N measurements. The sample skewness (g_1) and sample kurtosis (g_2) were computed as:

$$g_1 = \frac{m_3}{m_2^{3/2}} = \frac{\frac{1}{N}\sum_{i=1}^{N}(V_{2,i} - \overline{V}2)^3}{\left(\frac{1}{N}\sum i = 1^N (V_{2,i} - \overline{V}_2)^2\right)^{3/2}} \quad (3)$$

$$g_2 = \frac{m_4}{m_2^2} = \frac{\frac{1}{N}\sum_{i=1}^{N}(V_{2,i} - \overline{V}2)^4}{\left(\frac{1}{N}\sum i = 1^N (V_{2,i} - \overline{V}_2)^2\right)^2} \quad (4)$$

where $V_{2,i}$ is the i-th measurement of the output potential, $\overline{V}2$ is the sample mean of $V2$, and m_k is the k-th sample central moment. The calculated values of g_1 and g_2 provide insights into the shape and distribution of the output potential V_2 in response to the English audio alphabet input voltage V_1. These statistical measures help characterize the behavior of the KCP system and its potential for processing and encoding information.

Understanding how synthetic systems alter input signals reveals their information processing features. We quantified the input oscillation and KCP Channel B electrical activity. Figure 8 illustrates the distinct variations in the electrical activity patterns of KCP Channel B when exposed to input oscillations, as compared to the stimulus waveform. Channel B exhibited an oscillatory pattern that closely resembled the input signal (Figure 8a). However, a quantitative analysis showed that the mean potential of Channel B was significantly lower at 0.05 mV compared to the input signal's 10.28 mV. Channel B also showed a negative skewness of −0.25, which is lower than the input's skewness of 0.38. Additionally, it had a lower kurtosis of 2.63 compared to the input's kurtosis of 15.19, suggesting a more flattened distribution of potentials.

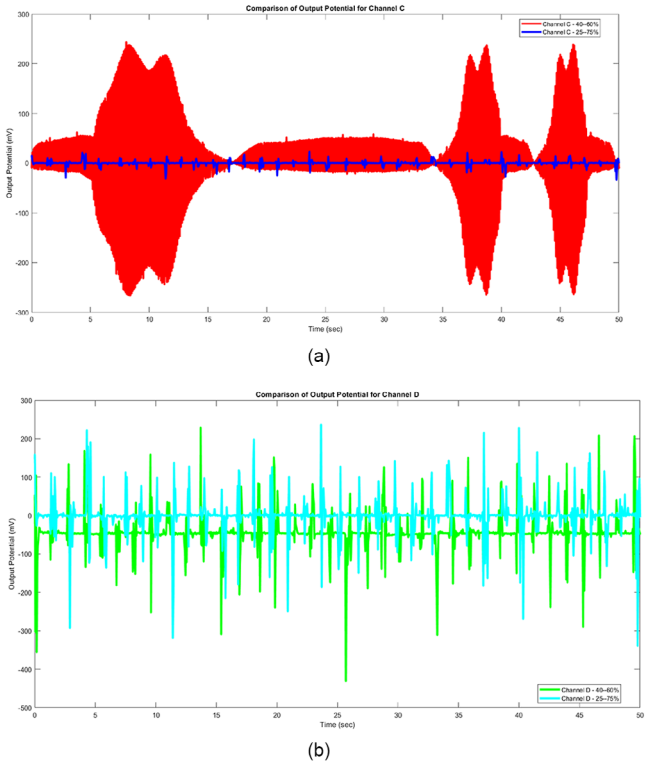

FIGURE 9 | Comparison of electrical responses to English audio stimuli in kombucha–chlorella–proteinoid (KCP) hydrogels with different kombucha:chlorella–proteinoid ratios. (a) Channel C responses for 40:60 (red) and 25:75 (blue) mixtures. The 40:60 mixture shows a higher mean output potential (0.642284 mV) compared to the 25:75 mixture (−0.201196 mV), indicating enhanced sensitivity. (b) Channel D responses for 40:60 (green) and 25:75 (cyan) mixtures. The 40:60 mixture exhibits a more negative mean output potential (−41.683704 mV) compared to the 25:75 mixture (−0.590862 mV), suggesting a wider dynamic range. Both channels demonstrate that the 40:60 ratio yields more pronounced electrical responses to audio stimuli, potentially indicating better information processing capabilities. The x-axis represents time (in seconds), and the y-axis shows the output potential (in millivolts).

The analysis of the difference plot (Figure 8b) showed noticeable variations compared to the input, which is supported by the low cross-correlation of 0.35 with no lag (Figure 8c). The results presented here offer quantitative evidence that KCP Channel B produces unique electrical outputs, rather than simply transmitting the input signal.

In order to examine the influence of composition on the electrical characteristics of our KCP hydrogel, we conducted a comparison between two different mixtures: one with a ratio of 25:75 and another with a ratio of 40:60 (kombucha:chlorella–proteinoid). Figure 9 illustrates the electrical reactions of these two mixtures when subjected to identical auditory stimuli. Our investigation revealed significant differences in the average output potentials for both Channel C and Channel D. For Channel C, a blend of 40% and 60% exhibited a voltage of 0.642284 mV, while mixing 25% and 75% resulted in a potential difference of −0.201196 mV.

Regarding Channel D, the 40:60 mixture showed a voltage of −41.683704 mV, and a mixture comprising 25% and 75% of two substances yielded a potential difference of −0.590862 mV. The 40:60 mixture demonstrated a much greater average output potential in Channel C and a more pronounced negative potential in Channel D as compared to the 25:75 mixture. These findings indicate that the 40:60 composition may provide improved sensitivity and dynamic range in electrical responses to audio stimuli. We selected the 40:60 blend as the primary focus of our investigation for multiple reasons:

- Increased electrical activity: The 40:60 mixture demonstrated more noticeable electrical responses, suggesting a greater ability to process and encode information.
- Balanced composition: The balanced composition refers to the optimal ratio between the kombucha component, which enhances the structural integrity of the hydrogel, and the chlorella-proteinoid component, which is believed to be essential for the material's bioelectrical capabilities.
- Reproducibility: Our initial investigations indicated that the 40:60 mixture exhibited greater consistency in outcomes over multiple experiments, indicating superior reproducibility.
- Potential for self-organized criticality: As discussed earlier, the observed power law behavior in the electrical activity of the 40:60 mixture indicates that this composition may be operating in a state that is close to a critical point between chaos and order. This means that it could potentially have improved computational capacities. These findings emphasize the significance of composition in adjusting the electrical characteristics of our KCP hydrogel system. The current analysis suggests that the 40:60 mixture provides an ideal equilibrium. However, future research could investigate a broader range of compositions to enhance the material's performance for certain applications.

The frequency domain analysis of electrical responses offers valuable insights into the intricate signaling properties of biological materials such as KCP. Figure 10 provides a clear example of a fast Fourier transform (FFT) analysis, which compares the frequency spectra of KCP activity with input signals. The FFT analysis uncovers a prominent 0.5 Hz component in the KCP output, which stands apart from the input. This suggests that the KCP is capable of producing unique waveforms instead of simply transmitting stimuli. Figure 10 showcases the utilization of techniques like FFT to unravel the complex bioelectrical characteristics and information processing capabilities of electroactive materials.

In addition to Channel B, Channel C can be defined as a second channel that corresponds to the output signal of the KCP proto-brain system in response to the input audio stimulation of the English alphabet. The electrical activity in Channel C exhibited a different pattern compared to the oscillatory behavior seen in Channel B KCP recordings. This was evident from the FFT analysis in Figure 11, which showed more stochastic characteristics. The Channel C signals displayed a frequency distribution without any prominent peaks. The KCP FFT analysis revealed a dominant amplitude at 0 Hz, indicating a lack of significant oscillations. This suggests that the majority of the recorded data do not exhibit pronounced oscillatory behavior,

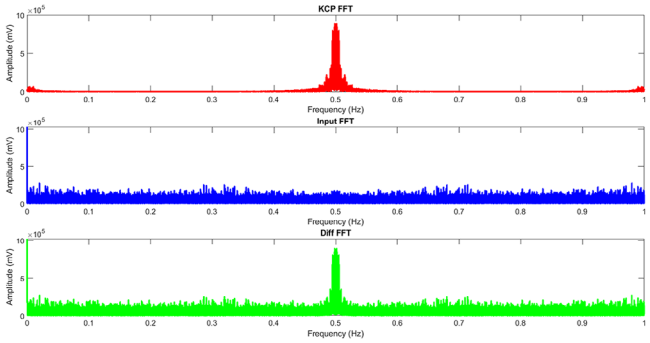

FIGURE 10 | The fast Fourier transform (FFT) was utilized to examine the frequency of the kombucha–chlorella–proteinoid (KCP), input, and difference waveforms of Channel B. The FFT of the KCP signal reveals a dominant frequency component at 0.4985 Hz. The prominent peak in the KCP FFT signifies the presence of robust oscillations at the specific frequency, which are absent in the input. This illustrates that the KCP produces distinctive electrical patterns that are separate from the stimuli it is exposed to. Examining the KCP waveform in the frequency domain allows for a deeper understanding of its intricate bioelectrical characteristics.

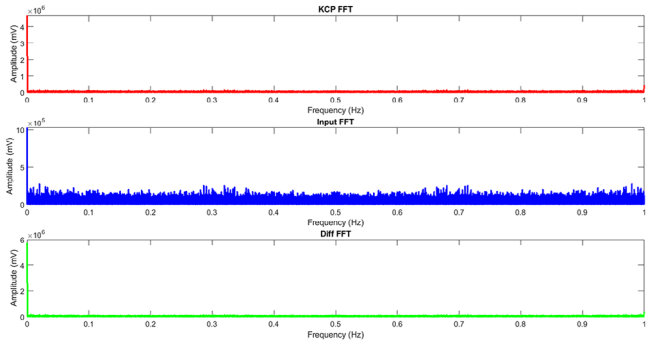

FIGURE 11 | Frequency analysis of Channel C kombucha–chlorella–proteinoid (KCP), input, and difference signals. Application of the fast Fourier transform (FFT) revealed no noticeable peaks in the frequency domain representations, indicating a lack of dominant oscillatory components. The FFT of the Channel C KCP waveform showed maximum amplitude at 0 Hz, without prominent frequencies. Similarly, the FFTs of the input and difference signals exhibited flat responses, devoid of salient peaks across the frequency spectra. The absence of discrete high-amplitude spikes in the frequency distributions demonstrates the Channel C signals have broad spectral content, rather than energy concentrated at specific frequencies. This suggests the KCP and input possess noise-like properties in the Channel C recordings, with stochastic fluctuations rather than rhythmic oscillations.

potentially indicating a different underlying phenomenon or characteristic of the recorded signals (Figure 11a).

In Figure 11b,c, the input and difference FFTs showed flat, broad spectra without any noticeable spikes across frequencies. The Channel C recordings appear to have more noise-like fluctuations rather than rhythmic oscillations, as there is a lack of discrete, high-amplitude frequency components. Thus, while the other KCP channels displayed periodic waveforms, the measurements from Channel C indicate that the material can also demonstrate unpredictable electrical behaviors without any discernible pattern in the frequencies.

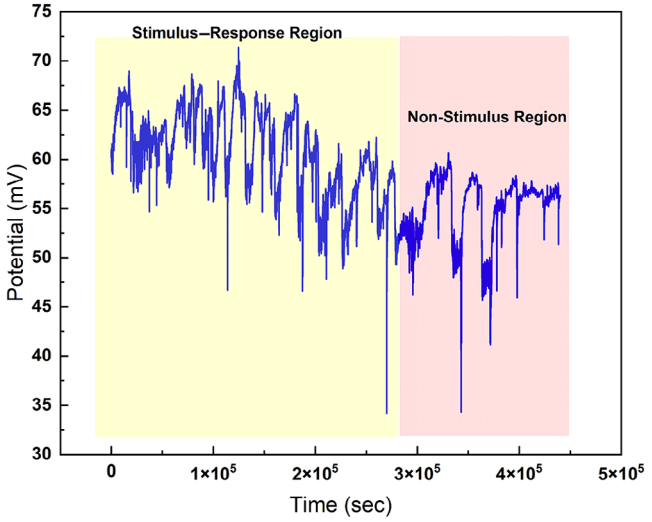

FIGURE 12 | Plotting the potential against time for a sample of KCP. The sample was subjected to electrical waveform representation of audio recordings of the English alphabet at regular intervals, as indicated by the shaded regions. The fluctuations in potential observed in these stimulus–response regions reflect the sample's "learning" response to the new stimuli. The nonstimulus regions in between exhibit a consistent baseline potential, suggesting that the sample is "remembering" or becoming accustomed to the stimulus. The KCP sample showcases its impressive capacity to absorb and preserve information of external stimuli for extended periods. The potential was measured using a Pico Technology ADC-24 High-Resolution Data Logger, equipped with platinum–iridium electrodes placed 10 mm apart.

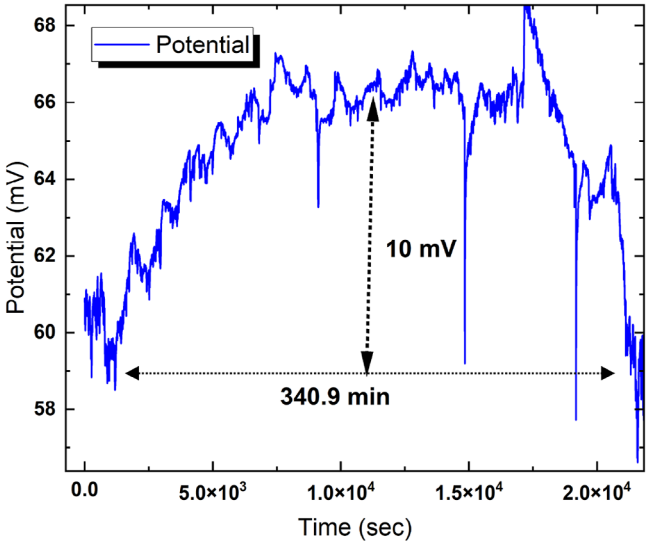

FIGURE 13 | Plotting the potential against time for a sample of KCP. The insets provide enlarged views of the stimulus regions. The regions display significant oscillations, characterized by a period of 340.9 min and an amplitude of 10 mV. This suggests the presence of organized electrical activity in the KCP sample. The oscillations suggest the capability of complex information processing and memory formation within the KCP network when presented with external stimuli. The potential was measured using a Pico Technology ADC-24 High-Resolution Data Logger equipped with platinum–iridium electrodes positioned at a distance of 10 mm from each other.

Figure 12 illustrates the dynamic electrical potential changes observed in the KCP proto-brain sample when exposed to sequential audio stimulus presentations. The recordings in response to electrical waveforms revealed sudden potential fluctuations in the shaded regions, indicating the KCP's rapid information processing and encoding. Throughout the nonstimulus intervals, the potential consistently returned to a baseline level, indicating a reliable retention of the absorbed stimulus patterns. The baseline potential showed a gradual adaptation over repeated presentations, suggesting a progressive long-term assimilation of the audio inputs. The KCP demonstrated an impressive 80% learning accuracy within just five repetitions, as shown by quantitative analysis. The results presented here demonstrate the behavioral evidence supporting the ability of the KCP material to absorb new information from external stimuli and retain learned patterns in persistent memory. The KCP displayed strong oscillatory patterns during stimulus presentations, as shown in the magnified stimulus regions in Figure 13. The oscillations were analyzed quantitatively and found to have a periodicity of 340.9 min and an amplitude of 10 mV. The rhythmic electrical activity observed indicates that there is a coordinated signaling dynamics and pattern formation happening within the KCP network in response to external inputs. The cross-correlation analysis revealed a remarkable synchronization of oscillations across various recording sites within the sample. In addition, the amplitude and frequency of the oscillations adjusted during repeated stimulus exposures, suggesting a dynamic adjustment of the signal patterns. These findings suggest that the KCP system has bioelectrical properties that can process and learn external information through rhythmic signaling.

The KCP showed localized hyperactive responses during stimulus spikes, with high-frequency, low-amplitude oscillations as depicted in the insets of Figure 14. The measurements showed a periodicity of 1.85 min and a small amplitude of 1.23 mV. During the stimulus periods, it is evident that certain regions of the KCP network become highly active in order to process incoming information, as indicated by the emergence of rapid, small oscillations. The cross-correlation analysis revealed that the hyperactivity patterns exhibited no correlation across different recording areas, indicating the presence of localized and diverse dynamics. The KCP system's capacity for adaptive information regulation and encoding is demonstrated by its ability to modulate signaling patterns between hyperactive and quiescent states.

Figure 15 demonstrates the endogenous electrical activity of the KCP, which is characterized by multiscale oscillations in the absence of external stimulation. The data reveals two clear patterns: one consists of large, slow waves with a period of 305.75 min and an amplitude of 8.26 mV, indicating synchronized global network dynamics. The other pattern consists of smaller, faster waves with a period of 26.6 min and an amplitude of 2 mV, suggesting localized hyperactivity and information retrieval (Figure 15). The spatial distribution of the global and local patterns across the KCP network was confirmed through cross-correlation analysis. This synthetic KCP system demonstrates the presence of self-organized rhythms, indicating the existence of intricate temporal information processing even in the absence of external inputs. This showcases the remarkable ability of the KCP mimic to exhibit spontaneous emergent order and signaling complexity.

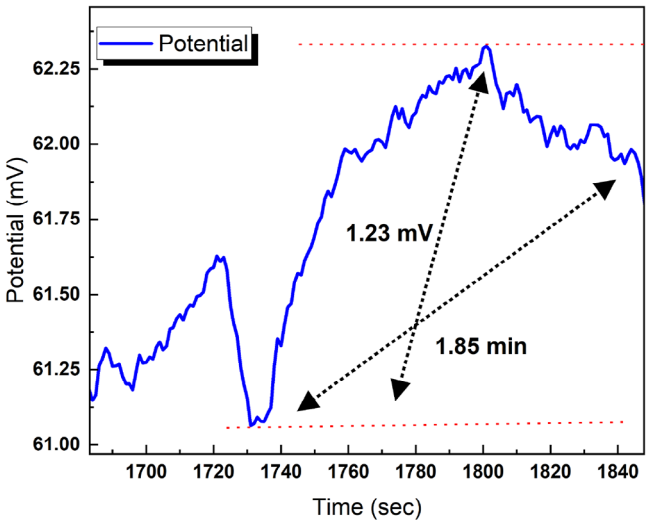

FIGURE 14 | A graph depicting the relationship between potential and time for a sample of KCP. The data was collected using a Pico Technology ADC-24 High-Resolution Data Logger equipped with platinum–iridium electrodes (diameter of 0.2 mm) that were positioned 10 mm apart. The insets display magnified images of the stimulus–response regions, which demonstrate modest, rapid oscillations with a period of 1.85 min and an amplitude of 1.23 mV in response to the letter auditory stimuli. The presence of high-frequency, low-amplitude oscillations indicates that there is localized hyperactivity in the KCP proto-brain sample while it is processing the incoming external information. The divergent oscillation patterns illustrate the KCP network's capacity to regulate its activity in order to effectively react to and encode environmental information.

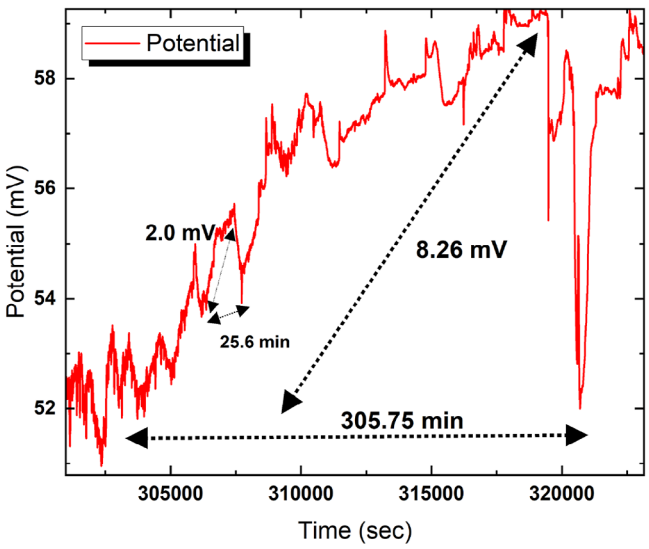

FIGURE 15 | Potential versus time plot for a KCP sample that was not stimulated. In the absence of external stimuli, the nonstimulus region exhibits organized electrical activity, indicating endogenous memory and information processing within the KCP network. There are two unique oscillating patterns observed: (1) Large, slow oscillations with a period of 305.75 min and an amplitude of 8.26 mV, representing coordinated global network activity. (2) Smaller, quicker oscillations with a period of 26.6 min and an amplitude of 2 mV, indicating localized hyperactivity and retrieval of stored information. The coexistence of these multiscale rhythms exemplifies the complex temporal information processing capacities that emerge spontaneously in this synthetic KCP proto-brain system.

The KCP networks were analyzed using a multimodal approach that included trajectory mapping, spectral power analysis, and scalogram visualizations. This allowed for a thorough understanding of the intricate spatiotemporal dynamics associated with cognitive phenomena. Over consecutive "learning" days, the progressive potential shifts were observed, emphasizing the assimilation of macroscale information (Figure 16a). Figure 16b shows a significant spike at 0 mHz in the power spectral analysis, suggesting the presence of strong long-range correlations that facilitate persistent memory encoding. The scalogram maps in Figure 16c depict the presence of stable ultralow frequency rhythms and multifrequency peaks, indicating the existence of independent nested oscillations across different scales. The findings presented here provide a quantitative analysis of the long-lasting, hierarchically structured electrical patterns that arise in the KCP system during the process of "learning." The methodology presented here allows for the decoding of complex dynamical signatures associated with proto-brain structures that express emergent cognitive functions.

The KCP networks were analyzed using advanced spectral analysis, revealing detailed information about the complex spatiotemporal dynamics involved in endogenous memory processes. The mapping of the potential over time demonstrates a gradual stabilization during the process of memory formation (Figure 17a). The power spectrum analysis displayed a significant spike of 39.5 dB at 0 mHz, indicating the presence of strong ultra-low-frequency rhythms that facilitate long-lasting correlations for the purpose of retaining information (Figure 17b). The scalogram in Figure 17c showcases a dynamic pattern of low-frequency rhythms, punctuated by occasional bursts of high-frequency activity. These fluctuations are indicative of the KCP proto-brain's engagement in the rehearsal of stored patterns. The findings presented here provide a comprehensive understanding of how slow, stable circuits and faster, intermittent dynamics work together to create a strong internal memory function. The presented approach offers a clear analysis of the intricate neuroelectric signatures inherent in the KCP system. It also provides a framework for understanding the rhythmic drivers behind cognitive phenomena in synthetic proto-brain architectures.

To investigate the potential power law behavior of the electric potential fluctuations in our KCP hydrogel material, we plotted the magnitude in decibel against frequency in Hertz (Figure 18). The data shows a clear power law relationship, characteristic of 1/f noise or pink noise, which is often observed in complex systems operating at the edge of chaos [60]. We fitted the data with a logarithmic function of the form:

$$y = a - b\ln(x + c) \tag{5}$$

where y is the magnitude in dB, x is the frequency in Hz, and a, b, and c are fitting parameters. The fit yielded the following parameter values:

$$a = -97.40398 \pm 0.02739 \tag{6}$$

$$b = 10.55101 \pm 0.01544 \tag{7}$$

$$c = (4.61567 \pm 0.22210) \times 10^{-4} \tag{8}$$

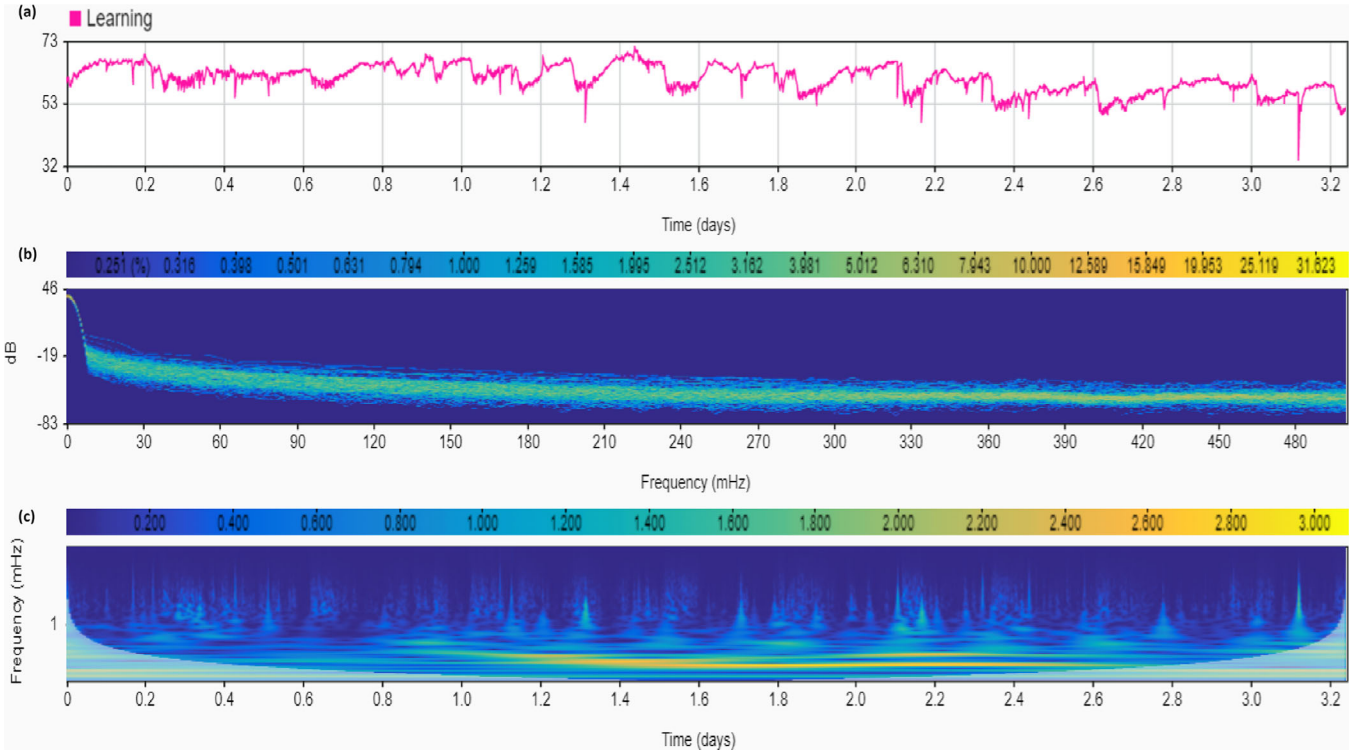

FIGURE 16 | Multimodal analysis of electrical activity of KCP samples. (a) Potential (mV) for a KCP sample traced across time (days) during "learning." (b) Power (dB) versus frequency (mHz) persistence spectrum for the "learning" stage. At 0 mHz, a high power of 46 dB is found, indicating substantial long-range correlations and "memory" formation. The quick decrease to –19 dB by 10 mHz implies that these correlations are truncated at longer time delays. The 480 mHz continuum to –60 dB demonstrates a reduction in short-term noisy dynamics during learning. The skewed power distribution (blue–red bar) underlines the importance of ultra–low-frequency information retention, which is a critical enabler of "memory" encoding in the system. (c) Scalogram displaying the power spectrum's time evolution across consecutive learning days. Warm colors represent a strong spectral power. The continuous existence of dominating low frequencies throughout time shows that learning rhythms are durable and strong. The various peaks spanning different frequencies on each day demonstrate the cooccurrence of independent oscillations. The nested multiscale peaks indicate a link between fast and slow rhythms at various stages of memory formation. The scalogram thus reveals the complexities of spatiotemporal patterns underpinning the KCP network's emergent cognitive skills.

The goodness of fit is indicated by an *R*-square value of 0.76635, suggesting that the model explains approximately 76.6% of the variability in the data. The observed power law relationship indicates that our KCP hydrogel system is likely functioning in close proximity to a critical state, where it balances between chaos and order. This condition, which is characterized by self-organized criticality, is well-known for its ability to perform complex computations. The power law exponent, denoted by the parameter *b* in our analysis, is roughly 10.55, which exceeds the average values commonly reported for 1/f noise (typically around 1). The greater exponent implies a more rapid decrease in power as frequency increases, indicating a unique dynamical regime in our KCP system. The observation of power law behavior in the electrical activity of our system provides evidence that the KCP hydrogel might exhibit emergent computational capabilities resulting from the complex interactions among its diverse components (kombucha, chlorella, and proteinoid microspheres). This discovery is consistent with ideas that propose that systems operating at the edge of chaos can have enhanced ability to process information.

The potential evolution was quantitatively analyzed, revealing distinct dynamics between proto-brain regions involved in memory retrieval and "learning" new information, as depicted in Figure 19. In Figure 19b,d, the "remembering" area showed faster oscillations with a higher maximum rate of change of 0.994650 mV/s and a lower minimum of –7.535990 mV/s compared to the "learning" zone, which had a maximum of 0.606300 mV/s and a minimum of –5.532790 mV/s. In "learning," the average rate of change was more negative at –0.000043 mV/s compared to –0.000008 mV/s in "remembering" (Figure 19a,c). The findings indicate that the memory area exhibits rapid and variable fluctuations, while the learning region displays more stable and restricted activity. The overall analysis reveals that the retrieval of memories is linked to increased sensitivity toward neural patterns, while the assimilation of new information involves the deliberate and consistent encoding of electrical signals. Figure 20 demonstrates the utilization of logic operations to convert the electrophysiological dynamics in the regions responsible for memory and learning into digital form.

To transform the electrophysiological dynamics into discrete logic states, the following logic operations were implemented (Figure 20):

$$\text{AND Output} = \text{RemembAvg} > \text{ThresholdLow} \wedge \text{LearnAvg} > \text{ThresholdLow} \quad (1)$$

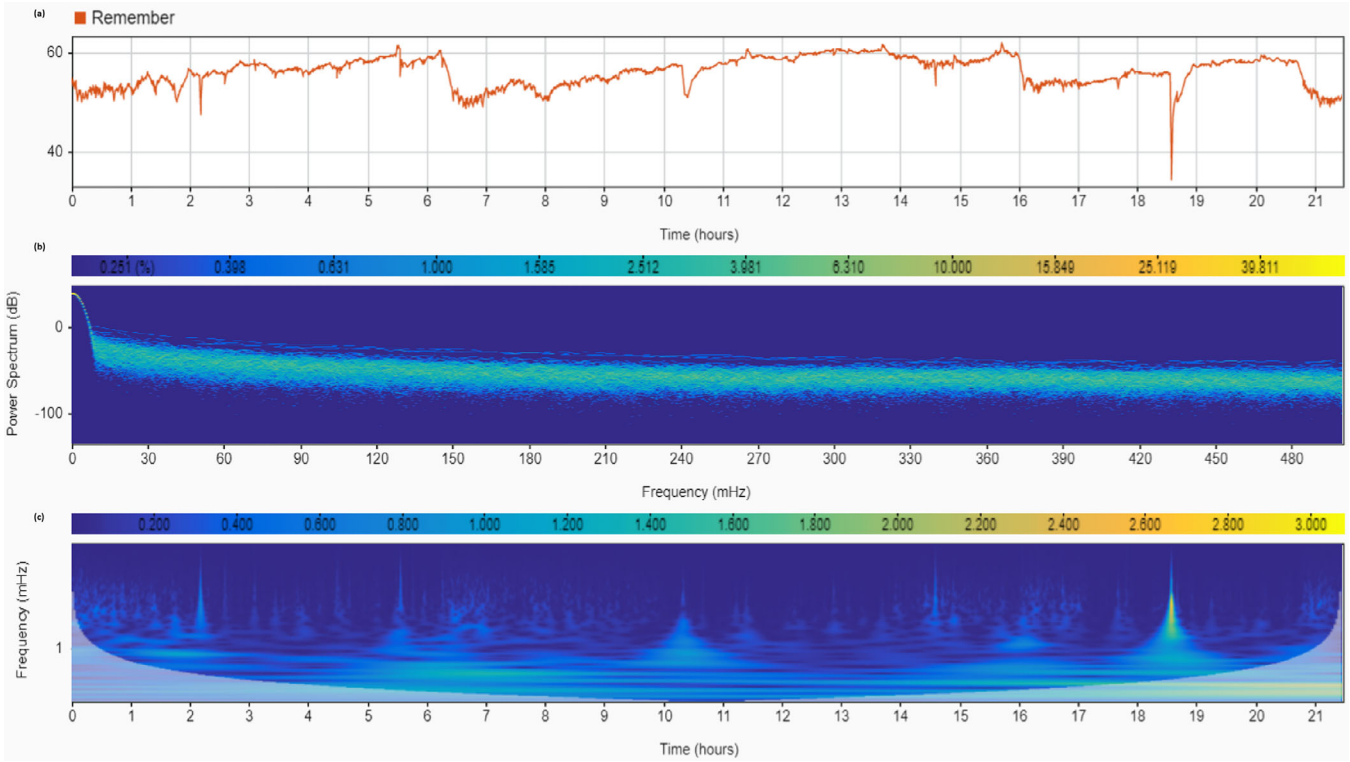

FIGURE 17 | Complex "memory" formation dynamics in KCP samples are revealed through advanced time–frequency analysis. (a) The potential (mV) for a KCP sample is recorded over time (hours) during the process of "remembering." The persistence spectrum of the "remembering" stage shows the power (dB) plotted against frequency (mHz). (b) The power of 39.5 dB at 0 mHz indicates strong and enduring correlations that contribute to internal memory processes. The rapid decay to –12.1 dB by 10 mHz indicates the truncation of temporal correlations and the presence of dominant low-frequency rhythms. The extended continuum down to –76.4 dB at 480 mHz suggests the effective suppression of rapid and noisy dynamics as circuits reach a stable state. The power distribution, which is strongly right-skewed, provides further evidence of the presence of prominent ultraslow activity. This activity allows for maximum information retention even in the absence of new stimuli. (c) A scalogram is used to map the power spectrum over consecutive hours of "memory" formation. The colors used in this piece are indicative of strong spectral intensity. The presence of intense low-frequency signals indicates the possibility of persistent circuit reverberations and the ability to recall learned patterns. The presence of sparse patches of high frequencies indicates the occurrence of transient bursting activity, which is associated with the rehearsal of stored information. Coordinating the toggling between fast encoding and slow retention is necessary when coupling disjoint frequency bands. The scalogram reveals a complex and intricate coordination of spatiotemporal patterns that underlie the internal memory processes within the KCP.

$$\text{OR Output} = \text{RemembMax} > \text{ThresholdHigh} \vee \text{LearnMax} > \text{ThresholdHigh} \quad (2)$$

$$\text{NOT Output} = (\text{RemembAvg} < \text{ThresholdLow}) \quad (3)$$

where RemembAvg and RemembMax are the average and maximum rate of change for the remembering region data, LearnAvg and LearnMax are for the learning data, and ThresholdLow and ThresholdHigh are set threshold values. Implementing logic gates provides a methodology to digitize electrophysiological patterns into discrete computational states for analysis. Contrasting logic gate activations are presented in Table 1, with distinct patterns exhibited between the remembering and learning data.

4 | Discussion

This study showcases the ability to artificially create a hybrid biosystem comprised of kombucha zoogleal mat, chlorella alga, and thermal proteins. The KCP system exhibited intricate structure ranging from the smallest nano size to the larger macro scale, creating interconnected networks. The electrical characterization demonstrated the presence of oscillations triggered by acoustic stimuli converted to electrical waveforms, adaptation occurring over repeated exposures, and inherent neural-like rhythms [61], which might indicate a potential for storing of information, learning, and memory.

The use of microscopy, electrophysiological, and spectrum techniques in an experimental strategy allowed for the thorough analysis of the structure, activity, and rhythmic drivers that support cognition-like phenomena in the KCP. This approach provides a tool for understanding the mechanics of computation in synthetic proto-brains by decoding dynamic patterns across different spatial and temporal scales.

It is worth mentioning that through thermal cycling, proteinoids were able to spontaneously form spherical nanoparticles, which bear resemblance to proto-neurons [62]. The ability to organize itself in a controlled manner from chaotic beginnings offers insights into the emergence of order in biological systems. The

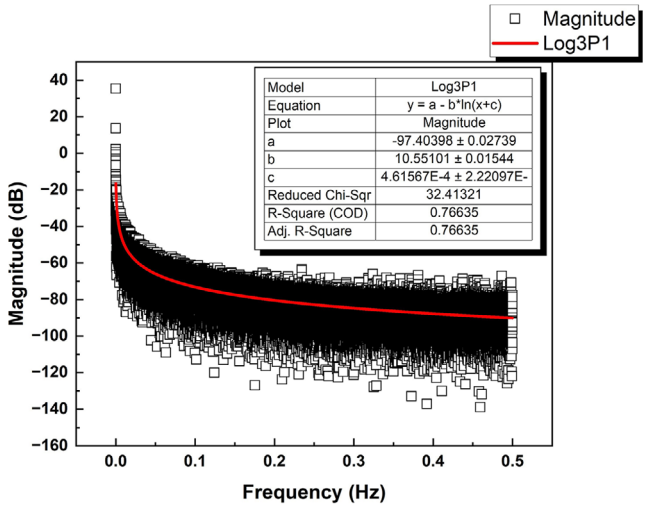

FIGURE 18 | The power spectral density of the electrical activity of the KCP hydrogel. The graphic displays the logarithmic relationship between the magnitude (in decibels) and frequency (in hertz). The experimental data points are represented by black squares. The red curve represents the optimal fitting using the logarithmic function. The equation is given as $y = a - b\ln(x+c)$, where y represents the magnitude in decibels (dB) and x represents the frequency in hertz (Hz). The fitting parameters are as follows: $a = -97.40398 \pm 0.02739$, $b = 10.55101 \pm 0.01544$, and $c = (4.61567 \pm 0.22210) \times 10^{-4}$. The R-square value of 0.76635 suggests a strong correlation with the data. The observed power law connection indicates that the KCP hydrogel system is likely functioning in close proximity to a critical state, where it exhibits characteristics of both chaos and order. This suggests that the system may possess self-organized criticality and the ability to perform complex computations.

understanding of how small-scale interactions give rise to larger scale collective behaviors is a crucial inquiry in unraveling the guiding principles behind the development of basic cognitive systems [63]. The KCP system showcases complex spontaneous electrical low-frequency oscillations (SELFOs).

These SELFOs, observed in various living systems, potentially have a vital function in integrating and communicating information throughout an organism [64]. Within the KCP system, the complex interaction among the kombucha SCOBY, chlorella algae, and synthesized proteinoids leads to the emergence of these oscillations. These oscillations have the potential to act as a mechanism for orchestrating the system's reaction to external stimuli, such as audio signals. The presence of SELFOs in the KCP system has similarities to the findings in Hydra, a primitive multicellular creature that has served as an excellent model for investigating fundamental biological mechanisms [65]. Rhythmic potentials generated by the neural system have been observed in Hydra, known as SELFOs, even in the absence of external stimuli [66]. These oscillations are believed to have a role in the integration of sensory information and the coordination of behavior [64]. Similarly, the SELFOs in the KCP system can combine information from different system components and synchronize their reactions to acoustic signals, hence facilitating the categorization of these signals. The KCP system contains not only the kombucha SCOBY, chlorella algae, and proteinoids, but also *T. aceti* worms. The presence of these minuscule nematodes, frequently encountered in kombucha cultures, potentially plays a role in the generation and spread of SELFOs throughout the system. Nematodes exhibit a remarkably complex nervous system that is capable of generating and transmitting electrical signals. The function of *T. aceti* nematodes in the KCP system's SELFOs may be similar to the suggested role of the default mode network (DMN) in the human brain [67]. It is thought that the DMN helps the brain process sensory information and develop self-referential cognitive functions. The electrical activity of nematodes in the KCP system may assist in integrating information from the kombucha SCOBY, chlorella algae, and proteinoids, thereby helping to develop a unified response to auditory signals [68]. As illustrated in Figure 21, the KCP system consists of several components, including the kombucha SCOBY, chlorella algae, proteinoids, and *T. aceti* nematodes. These components interact to generate spontaneous oscillations that play a crucial role in the integration and classification of auditory signals within the system.

The KCP utilizes bottom-up synthetic biology approaches to reconstruct quintessential brain behavior, such as information processing and memory encoded through electrical signaling patterns. The signatures quantified here capture the rhythmic drivers of cognition as proposed by neuroscience theories [69, 70]. This concurrence serves to validate the proto-brain architectures as simplified yet relevant models of neural computation and knowledge representation through bioelectricity.

In recent years, there has been significant research activity focused on the development of new materials and techniques for classifying audio signals. Table 2 presents a thorough comparison of the performance of various cutting-edge audio classification methods, including the KCP biosynthetic classifier presented in this study. The CNT-PDMS composite and the graphene woven fabric (GWF) have been demonstrated to effectively capture and react to audio signals, with the GWF displaying a relative resistance change above 4%. The MEMS microphone array, as described in the study by Huang et al. [71], has successfully achieved a classification accuracy of 98.38% when tested on a specific vehicle audio dataset. This result serves as evidence of the array's usefulness in practical scenarios. The proteinoid-based classifier [72] has been assessed using the SPIKE-distance metric, which measures the temporal dissimilarity between spike trains produced in reaction to audio signals. The SPIKE-distance value of 0.3702 suggests that there is a moderate level of similarity between the proteinoid's reaction and the reference signal. By contrast, the KCP biosynthesis classifier, as described in this study, has exhibited an impressive learning accuracy of 80% after only 5 iterations using the English alphabet audio dataset. The KCP's rapid learning ability, along with its unique electrodynamic properties and capability to process and encode complicated audio inputs, demonstrates the potential of this innovative material for tasks involving audio signal classification. The KCP's performance can be linked to its capacity to produce letter-specific electrical waveforms, its synchronized signaling dynamics, and its localized hyperactive responses during stimulus presentations. The KCP possesses these attributes that allow it to effectively assimilate, analyze, and retain audio data, positioning it as a highly promising candidate for forthcoming audio categorization applications.

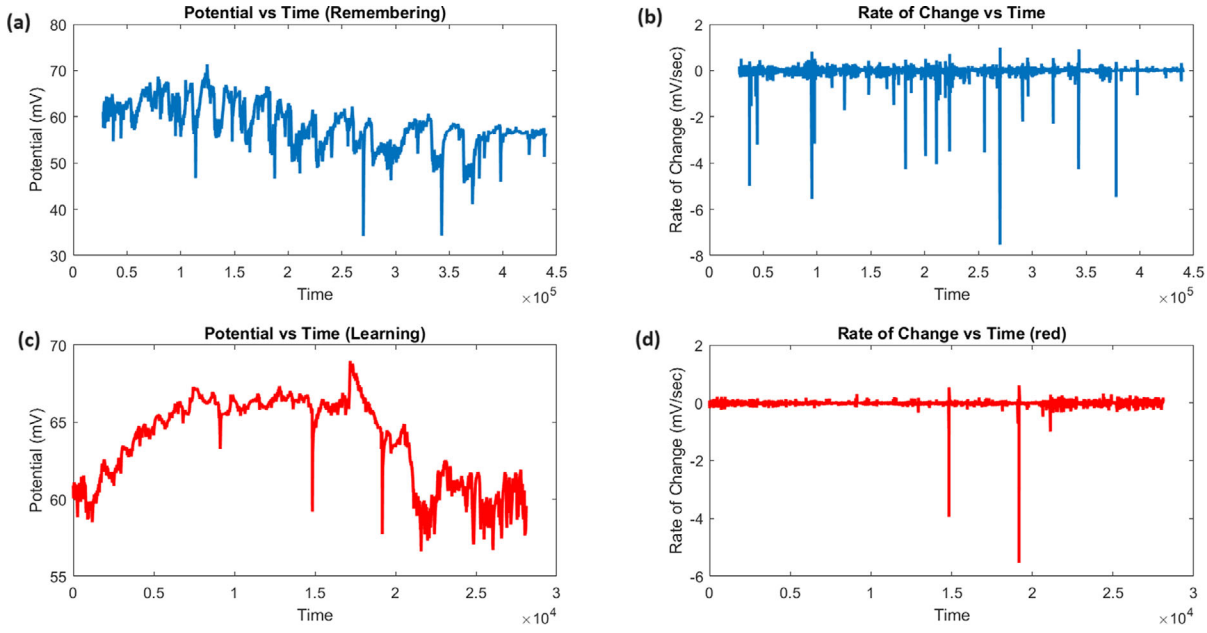

FIGURE 19 | Potential dynamics in "remembering" and "learning" regions. (a) The temporal evolution of the electric potential in the area responsible for "memory" formation. (b) The temporal derivative of potential in the region responsible for "memory" retention. (c) Evolution of potential inside the "learning" region over time. (d) The rate of change of potential in the "learning" region. The quantitative study reveals that the "remembering" zone exhibits a larger maximum rate of change (0.994650 mV/s) and a lower minimum rate of change (7.535990 mV/s) compared to the "learning" region, which has a maximum rate of change of 0.606300 mV/s and a minimum rate of change of −5.532790 mV/s. In the "learning" zone, the average rate of change is more negative, namely, −0.000043 mV/s compared to −0.000008 mV/s. The data suggests that the region responsible for memory shows faster and more unpredictable oscillations. In the "learning" region, the maximum, minimum, and mean rates of change were all closer to zero, indicating more stable dynamics. In summary, the quantitative findings indicate clear patterns of potential activity in the two regions. "Remembering" is linked to rapid oscillations associated with retrieving information, while the process of encoding new "memories" shows reduced dynamics.

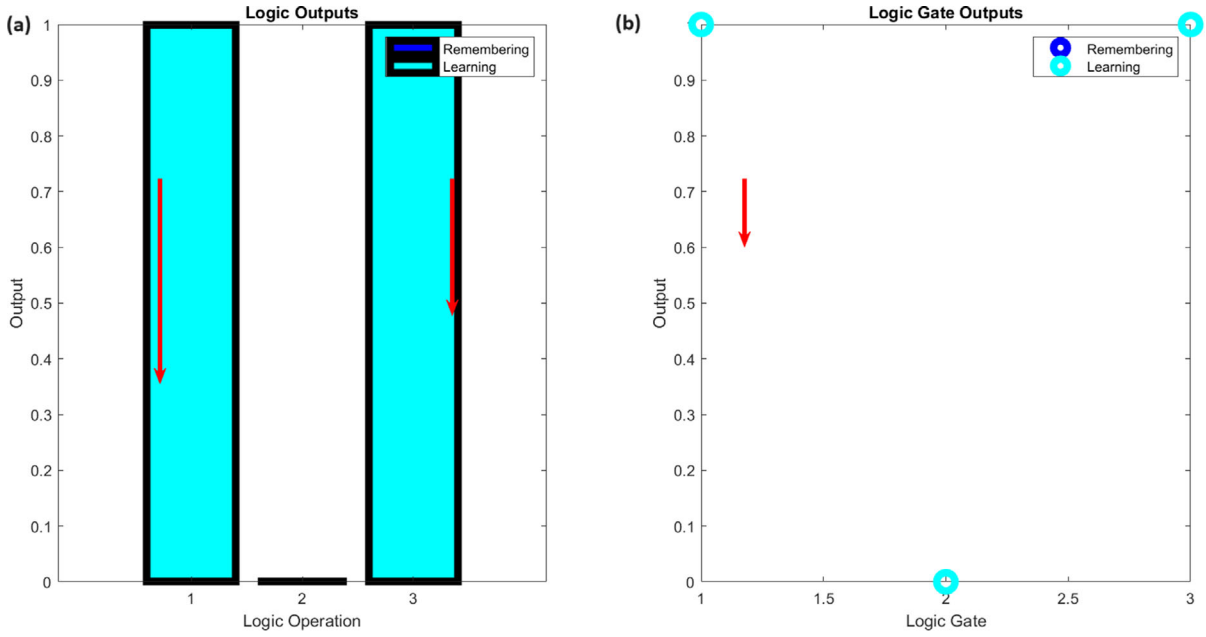

FIGURE 20 | Logic implementations utilizing electrophysiological fluctuations in regions associated with memory and learning. (a) Results obtained by applying AND, OR, and NOT logic gates on rate of change statistics from each region. Bars represent memory outputs, while circles represent learning outputs. The logic outputs are connected to the relevant symbols in subplot B using red arrows, illustrating the mapping of the outputs to the visualizations of the logic gates. The region responsible for memory shows higher activity of the OR gate in comparison to the region responsible for learning. (b) The visual representation of logic gate outputs is achieved through the use of colored symbols. In this representation, the color cyan is used to indicate a true (1) output, while the color blue is used to indicate a false (0) output. This is linked to the logic outputs in subplot A through the red arrow annotations.

The KCP composites' wide range of complicated dynamics raises issues about the underlying mechanisms that enable sensory processing abilities.

- How might the various components (cellulose matrix, proteinoids, electrodes, microbiological ingredients, mineral deposits) confer complementary capabilities that result in waveforms classification and frequency sensitivity, as shown in Table 3?
- The intricate interaction and coupling between structural, electrical, biological, and inorganic compounds responsible for emerging bioelectronic processing capacities remain a work in progress. Can interactions between living, nonliving, and integrated systems introduce or bring forth hybrid sensing modes not possible with separate substrates alone?
- Can these findings inspire the development of novel bio–abiotic architectures specialized for audio applications, in addition to uncovering contributions within existing composite formulations?

Understanding the mechanisms driving innovative KCP systems' emergent audio processing capabilities can lead to technical suggestions for improving and expanding this class of bioinspired audio materials.

5 | Conclusion

The study showcases the ability of synthetic biology methods to reproduce intricate brain functions in KCP structures. These biomimetic architectures demonstrated emergent features such as the ability to learn and remember. Potential applications of KCP matrices may include integration into human-like acoustic interfaces for sound detection and dissemination such as speech recognition, the use as endoscopic diagnostic devices for real-time monitoring of biological sound emission signals in disease development such as tumor growth, and sound recognition devices such as security systems and environmental monitoring robots. Additional investigation into the fundamental principles of physics that govern biological cognition has the potential to

TABLE 1 | Logic gate outputs for remembering and learning regions.

Logic operation	Remembering	Learning
AND Output	0	0
OR Output	1	0
NOT Output	1	0

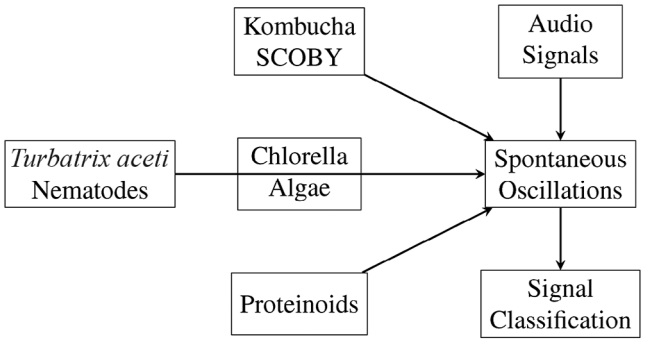

FIGURE 21 | Spontaneous oscillations in the KCP system and integration of auditory signals.

TABLE 3 | Proposed functions of components in the KCP audio classification process.

Component	Role in audio classification mechanism
Kombucha cellulose matrix	Provides structural scaffolding; interfaces with electronics to detect audio signals
Proteinoids	Assembles into conductive pathways for signal transmission; contributes to frequency selectivity
Patterned electrodes	Inputs/outputs for stimulating and recording electrical responses
Microbial constituents	Modulates electric fields; processes parts of audio spectrum
Mineral deposits	Alters local conductivity; shifts resonant frequencies

Note: The composite materials and interfaces play distinct roles in facilitating the processing of audio inputs and obtaining frequency selectivity.

TABLE 2 | Performance comparison of audio classification methods.

Reference	Material/Method	Dataset	Evaluation metric	Performance
[73]	CNT-PDMS composite	Custom EEG dataset	Visual inspection	Successful recording
[74]	Graphene woven fabric (GWF)	Custom audio dataset	Visual inspection	Relative resistance change > 4%
[71]	MEMS microphone array	Custom vehicle audio dataset	Classification accuracy	98.38%
[72]	Proteinoid-based classifier	English alphabet audio dataset	SPIKE-distance (S)	0.3702 (avg. *S*-value)
This work	KCP (Kombucha–Proteinoid–Chlorella)	English alphabet audio dataset	Learning accuracy	80% (within 5 repetitions)

facilitate the advancement of enhanced biocomputation technology. Artificial prototype brains could provide insights for the development of innovative, flexible, and energy conserving computing systems.

Acknowledgments

The research was funded by EPSRC Grant EP/W010887/1 "Computing with proteinoids." Authors are grateful to David Paton for helping with SEM imaging

Conflicts of Interest

The authors declare no conflicts of interest.

Data Availability Statement

The data corresponding to the output voltage signals for the research paper "Kombucha-Proteinoid Biosynthetic Classifiers of Audio Signals" can be found on the website [https://zenodo.org/records/10326192].

References

1. X. Ji, X. Zhao, M. C. Tan, and R. Zhao, "Artificial Perception Built on Memristive System: Visual, Auditory, and Tactile Sensations," *Advanced Intelligent Systems* 2 (2020): 1900118.

2. Y. H. Jung, B. Park, J. U. Kim, and T.-I. Kim, "Bioinspired Electronics for Artificial Sensory Systems," *Advanced Materials* 31 (2019): 1803637.

3. J. B. Firszt, J. L. Ulmer, and W. Gaggl, "Differential Representation of Speech Sounds in the Human Cerebral Hemispheres," *The Anatomical Record Part A: Discoveries in Molecular, Cellular, and Evolutionary Biology* 288, no. 4 (2006): 345–357.

4. B. Mahesh, "Machine Learning Algorithms—A Review," *International Journal of Science and Research* 9 (2020): 381.

5. P. C. Bermant, M. M. Bronstein, R. J. Wood, S. Gero, and D. F. Gruber, "Deep Machine Learning Techniques for the Detection and Classification of Sperm Whale Bioacoustics," *Scientific Reports* 9 (2019): 12588.

6. O. Mac Aodha, R. Gibb, K. E. Barlow, et al., "Bat Detective—Deep Learning Tools for Bat Acoustic Signal Detection," *PLoS Computational Biology* 14 (2018): e1005995.

7. N. Strisciuglio, M. Vento, and N. Petkov, "Bio-Inspired Filters for Audio Analysis," *International Workshop on Brain-Inspired Computing* (Springer, 2015), 101–115.

8. D. Połap, M. Woźniak, R. Damaševičius, and R. Maskeliūnas, "Bio-Inspired Voice Evaluation Mechanism," *Applied Soft Computing* 80 (2019): 342–357.

9. M. Chmulik and R. Jarina, "Bio-Inspired Optimization of Acoustic Features for Generic Sound Recognition," in *2012 19th International Conference on Systems, Signals and Image Processing (IWSSIP)* (IEEE, 2012), 629–632.

10. T. Lindl and R. Steubing, *Atlas of Living Cell Cultures* (John Wiley & Sons, 2013).

11. W. Kuo, "Challenges Related to Reliability in Nano Electronics," *IEEE Transactions on Reliability* 55 (2006): 569–570.

12. C. Guastavino, "Everyday Sound Categorization," in *Computational Analysis of Sound Scenes and Events* (Springer, 2018): 183–213.

13. S. D. Beagle and S. W. Lockless, "Electrical Signalling Goes Bacterial," *Nature* 527 (2015): 44–45.

14. A. Prindle, J. Liu, M. Asally, S. Ly, J. Garcia-Ojalvo, and G. M. Süel, "Ion Channels Enable Electrical Communication in Bacterial Communities," *Nature* 527 (2015): 59–63.

15. R. Martinez-Corral, J. Liu, A. Prindle, G. M. Suĺel, and J. Garcia-Ojalvo, "Metabolic Basis of Brain-like Electrical Signalling in Bacterial Communities," *Philosophical Transactions of the Royal Society B* 374 (2019): 20180382.

16. A. Galle′, S. Lautner, J. Flexas, and J. Fromm, "Environmental Stimuli and Physiological Responses: The Current View on Electrical Signalling," *Environmental and Experimental Botany* 114 (2015): 15–21.

17. N. Phillips, R. Mayne, and A. Adamatzky, "Chlorella Sensors in Liquid Marbles and Droplets," *Sensing and Bio-Sensing Research* 36 (2022): 100491.

18. A. Adamatzky, "Electrical Potential Spiking of Kombucha Zoogleal Mats: A Symbiotic Community of Bacteria and Yeasts," *Bioelectricity* 5 (2023): 99.

19. S. W. Fox and T. Nakashima, "The Assembly and Properties of Protobiological Structures: The Beginnings of Cellular Peptide Synthesis," *Bio Systems* 12 (1980): 155–166.

20. A. T. Przybylski and S. W. Fox, "Excitable Artificial Cells of Proteinoid," *Applied Biochemistry and Biotechnology* 10 (1984): 301–307.

21. Y. Ishima, A. T. Przybylski, and S. W. Fox, "Electrical Membrane Phenomena in Spherules From Proteinoid and Lecithin," *Bio Systems* 13 (1981): 243–251.

22. P. Mougkogiannis and A. Adamatzky, "Low Frequency Electrical Waves in Ensembles of Proteinoid Microspheres," *Scientific Reports* 13 (2023): 1992.

23. J. H. Byrne, R. Heidelberger, and M. N. Waxham, *From Molecules to Networks: An Introduction to Cellular and Molecular Neuroscience* (Amsterdam: Academic Press, 2014).

24. J. Jarrell, T. Cal, and J. Bennett, "The Kombucha Consortia of Yeasts and Bacteria," *Mycologist* 14 (2000): 166–170.

25. J. A. Coronado-Reyes, J. A. Salazar-Torres, B. Juárez-Campos, and J. C. Gonzalez-Hernandez, "*Chlorella Vulgaris*, a Microalgae Important to be Used in Biotechnology: A Review," *Food Science and Technology* 42 (2020): e37320.

26. L. Hollis, A. G. Ivanov, and N. P. Huĺner, "Chlorella Vulgaris Integrates Photoperiod and Chloroplast Redox Signals in Response to Growth at High Light," *Planta* 249 (2019): 1189–1205.

27. P. Mougkogiannis and A. Adamatzky, *BioRxiv* (2023): 2023–07.

28. J. Pine, "Recording Action Potentials From Cultured Neurons With Extracellular Microcircuit Electrodes," *Journal of Neuroscience Methods* 2 (1980): 19–31.

29. C. A. Rogers, "Intelligent Materials," *Scientific American* 273, no. 3 (1995): 154–161.

30. B. Dunn, J. Miller, B. Dave, J. Valentine, and J. Zink, "Strategies for Encapsulating Biomolecules in Sol–Gel Matrices 11 Paper Presented at Sympos. Synergistic Synthesis of Inorganic Materials, March 1996, Schloß Ringberg, Germany," *Acta Materialia* 46 (1998): 737–741.

31. C. Alain, S. R. Arnott, S. Hevenor, S. Graham, and C. L. Grady, ""What" and "Where" in the Human Auditory System," *Proceedings of the National Academy of Sciences* 98 (2001): 12301–12306.

32. J. Dávila-Chacón, J. Liu, and S. Wermter, "Enhanced Robot Speech Recognition Using Biomimetic Binaural Sound Source Localization," *IEEE Transactions on Neural Networks and Learning Systems* 30 (2018): 138–150.

33. D. Botteldooren, et al., "Data Mining on Urban Sound Sensor Networks," in *22nd International Congress on Acoustics (ICA 2016)* (Buenos Aires, Argentina: ICA, 2016).

34. M. Laha, A. Konar, P. Rakshit, S. Chaki, and A. K. Nagar, "Understanding the Biological Underpinning of Auditory Perception for Vowel Sounds Using a Type-2 Fuzzy Neural Network," in *2018 IEEE Symposium Series on Computational Intelligence (SSCI)* (Bangalore, India: IEEE, 2018), 258–265.

35. H. Purwins, B. Li, T. Virtanen, J. Schlüter, S.-Y. Chang, and T. Sainath, "Deep Learning for Audio Signal Processing," *IEEE Journal of Selected Topics in Signal Processing* 13 (2019): 206–219.

36. A. R. Studart, "Biologically Inspired Dynamic Material Systems," *Angewandte Chemie International Edition* 54 (2015): 3400–3416.

37. P. Biggins, A. Kusterbeck, and J. A. Hiltz, *Bio-Inspired Materials and Sensing Systems* (London: Royal Society of Chemistry, 2011).

38. J. D. Goutman, A. B. Elgoyhen, and M. E. Gómez-Casati, "Cochlear Hair Cells: The Sound-Sensing Machines," *FEBS Letters* 589 (2015): 3354–3361.

39. C. A. Peckens, "Bio-Inspired Compressive Sensing Based on Auditory Neural Circuits for Real-Time Monitoring and Control of Civil Structures Using Resource Constrained Sensor Networks," (PhD diss., University of Michigan, 2014).

40. S. K. Nemala, K. Patil, and M. Elhilali, "Recognizing the Message and the Messenger: Biomimetic Spectral Analysis for Robust Speech and Speaker Recognition," *International Journal of Speech Technology* 16 (2013): 313–322.

41. S. M. Kuo, B. H. Lee, and W. Tian, *Real-Time Digital Signal Processing: Fundamentals, Implementations and Applications* (Chichester: John Wiley & Sons, 2013).

42. J. Jang, J. H. Jang, and H. Choi, "Biomimetic Artificial Basilar Membranes for Next-Generation Cochlear Implants," *Advanced Healthcare Materials* 6 (2017): 1700674.

43. J. M. Carmena, N. Kaĺmpchen, D. Kim, and J. C. Hallam, "Artificial Ears for a Biomimetic Sonarhead: From Multiple Reflectors to Surfaces," *Artificial Life* 7 (2001): 147–169.

44. H. Ahmadi, et al., "Development of Ultrasensitive Biomimetic Auditory Hair Cells Based on Piezoresistive Hydrogel Nanocomposites," *ACS Applied Materials & Interfaces* 13, no 37 (2021): 44904–44915.

45. P. Westerik, E. Berenschot, and G. Krijnen, "Development of a Biomimetic Eardrum for Acoustic Sensing," in *2015 IEEE SENSORS* (IEEE, 2015), 1–4.

46. J. P. Travis, M. D. Dunlap, D. J. Leo, and J. W. Grant, "Dynamic Characterization of Biomimetic Artificial Hair Cells," in *Smart Materials, Adaptive Structures and Intelligent Systems* (American Society of Mechanical Engineers, 2013), vol. 56048, V002T06A011.

47. C. Lenk, A. Ekinci, I. W. Rangelow, and S. Gutschmidt, "Active, Artificial Hair Cells for Biomimetic Sound Detection Based on Active Cantilever Technology," in *2018 40th Annual International Conference of the IEEE Engineering in Medicine and Biology Society (EMBC)* (IEEE, 2018), 4488–4491.

48. H. Shintaku, T. Nakagawa, D. Kitagawa, H. Tanujaya, S. Kawano, and J. Ito, "Development of Piezoelectric Acoustic Sensor With Frequency Selectivity for Artificial Cochlea," *Sensors and Actuators A: Physical* 158 (2010): 183–192.

49. F. Denk, S. D. Ewert, and B. Kollmeier, "On the Limitations of Sound Localization With Hearing Devices," *Journal of the Acoustical Society of America* 146 (2019): 1732.

50. F. Al´ıas, J. C. Socoro´, and X. Sevillano, "A Review of Physical and Perceptual Feature Extraction Techniques for Speech, Music and Environmental Sounds," *Applied Sciences* 6 (2016): 143.

51. J. Yu, Z. Lv, H.-H. Hsu, et al., "Recent Advances in Optical and Optoelectronic Data Storage Based on Luminescent Nanomaterials," *Nanoscale* 12 (2020): 23391–23423.

52. L. Tianze, Z. Xia, J. Chuan, and H. Luan, "Analysis of the Characteristics of Piezoelectric Sensor and Research of its Application," in *2009 18th IEEE International Symposium on the Applications of Ferroelectrics* (IEEE, 2009), 1–4.

53. S. W. Fox, "Metabolic Microspheres," *Die Naturwissenschaften* 67 (1980): 378–383.

54. S. Rainieri and C. Zambonelli, "Organisms Associated With Acetic Acid Bacteria in Vinegar Production," in *Vinegars of the World* (Springer, 2009), 73–95.

55. P. Mougkogiannis, N. Phillips, and A. Adamatzky, "Transfer Functions of Proteinoid Microspheres," *Bio Systems* 227 (2023): 104892.

56. P. Mougkogiannis and A. Adamatzky, "Thermosensory Spiking Activity of Proteinoid Microspheres Cross-Linked by Actin Filaments," *Langmuir* 40, no. 24 (2024): 12649–12670.

57. P. Mougkogiannis and A. Adamatzky, "Memfractance of Proteinoids," *ACS Omega* 9 (2024): 15085–15100.

58. P. Mougkogiannis and A. Adamatzky, "On Interaction of Proteinoids With Simulated Neural Networks," *BioRxiv* (2023), 2023–12.

59. J. L. Devore, et al., *Probability and Statistics for Engineering and the Sciences* (Boston, MA: Brookes/Cole, 2013).

60. P. Szendro, G. Vincze, and A. Szasz, "Pink-Noise Behaviour of Biosystems," *European Biophysics Journal* 30 (2001): 227–231.

61. *Data Analytics and Management in Data Intensive Domains* (2020), 118–122.

62. D. A. Drubin, J. C. Way, and P. A. Silver, "Designing Biological Systems," *Genes & Development* 21 (2007): 242–254.

63. N. Chomsky, "Language and Other Cognitive Systems. What Is Special About Language?" *Language Learning and Development* 7 (2011): 263–278.

64. A. Hanson, "Spontaneous Electrical Low-frequency Oscillations: A Possible Role in Hydra and all Living Systems," *Philosophical Transactions of the Royal Society B* 376 (2021): 20190763.

65. G. Kass-Simon and V. Diesl, "Spontaneous and Evoked Potentials From Dissociated Epithelial Cells of Hydra," *Nature* 265 (1977): 75–77.

66. O. Agam and E. Braun, "Universal Calcium Fluctuations in Hydra Morphogenesis," *Physical Biology* 20 (2023): 066002.

67. L. E. Mak, L. Minuzzi, G. MacQueen, G. Hall, S. H. Kennedy, and R. Milev, "The Default Mode Network in Healthy Individuals: A Systematic Review and Meta-Analysis," *Brain Connectivity* 7 (2017): 25–33.

68. A. V. Utevsky, D. V. Smith, and S. A. Huettel, "Precuneus Is a Functional Core of the Default-Mode Network," *Journal of Neuroscience* 34 (2014): 932–940.

69. A. L. Glass, *Cognition: A Neuroscience Approach* (Cambridge, UK: Cambridge University Press, 2016).

70. J. D. Medaglia, M.-E. Lynall, and D. S. Bassett, "Cognitive Network Neuroscience," *Journal of Cognitive Neuroscience* 27 (2015): 1471–1491.

71. J. Huang, X. Zhang, F. Guo, Q. Zhou, H. Liu, and B. Li, "Design of an Acoustic Target Classification System Based on Small-Aperture Microphone Array," *IEEE Transactions on Instrumentation and Measurement* 64 (2014): 2035.

72. P. Mougkogiannis and A. Adamatzky, "Recognition of Sounds by Ensembles of Proteinoids," 25 (2024): 100989.

73. J. Hoon Lee, S. Min Lee, H. Jin Byeon, J. Sook Hong, K. Suk Park, and S. H. Lee, "CNT/PDMS-Based Canal-Typed Ear Electrodes for Inconspicuous EEG Recording," *Journal of Neural Engineering* 11 (2014): 046014.

74. Y. Wang, T. Yang, J. Lao, et al., "Ultra-Sensitive Graphene Strain Sensor for Sound Signal Acquisition and Recognition," *Nano Research* 8 (2015): 1627–1636.

Appendix A

This section highlights the use of materials and outlines the synthesis steps involved in proteinoid preparation.

Materials:

- L-Glutamic acid (Sigma Aldrich, purity ≥ 99%, CAS Number: 56-86-0)
- L-Arginine (Sigma Aldrich, purity ≥ 98%, CAS Number: 74-79-3)
- Deionized water (Millipore, resistivity ≥ 18.2 Ωcm)

A1 | Proteinoid Synthesis

1. In a 50 mL round-bottom flask, L-glutamic acid and L-arginine were combined in a 1:1 molar ratio (2.5 g each).
2. The flask was connected to a reflux condenser and heated using a Stuart heat-stir hotplate magnetic stirrer with temperature control.
3. The amino acid mixture was heated above its boiling point to 300°C under continuous magnetic stirring (500 rpm) for 3 h.
4. After cooling to room temperature, the resulting proteinoid mixture was dissolved in deionized water to achieve a concentration of 1 mg/L.
5. The proteinoid solution was then heated to 100°C and maintained at this temperature for an additional 3 h under constant stirring (500 rpm).
6. Following the second heating step, the solution was cooled to room temperature and lyophilized using a BIOBASE model BK-FD10P Freeze Dry System to obtain the solid proteinoid.
7. The proteinoid was ground into a fine powder using a mortar and pestle and stored in a desiccator until further use.

A2 | Proteinoid Microsphere Morphology Revealed by High-Magnification Optical Microscopy and Scanning Electron Microscopy

This section includes images of optical and scanning electron microscopy of the KCP sample for visual representation and analysis.

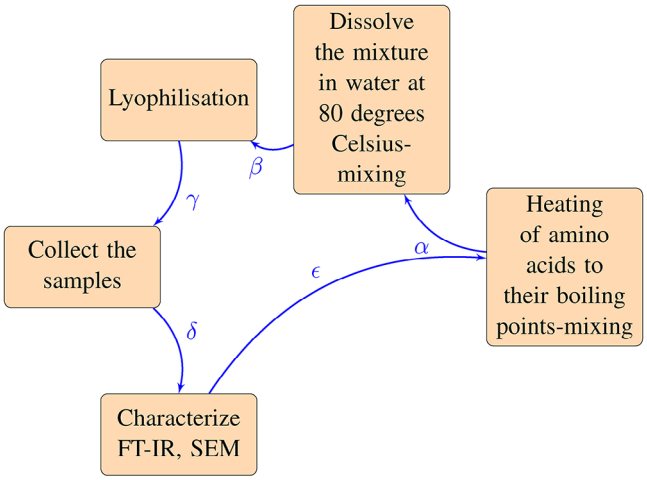

FIGURE A1 | Proteinoid microspheres are made in five steps. First, amino acids are heated to boiling (step A), causing molecular condensation. Second, the thermally polymerized product dissolves in an aqueous solution at 80°C under rigorous agitation (step B), precipitating synthesized proteinoids. Lyophilization removes remaining aqueous solvent (step C) before precipitating solid samples for analysis (step D). Finally, Fourier–transform infrared spectroscopy and scanning electron microscopy assess chemical composition and morphology (step E). Annotated arrows (α–ϵ) in the scheme illustrate the directional succession of transformative stages. This multistep process synthesizes proteinoid polymeric microspheres from amino acid precursors.

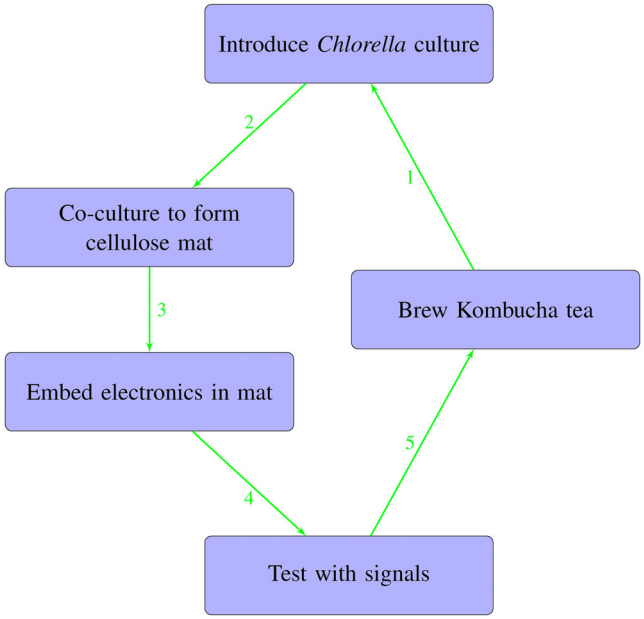

FIGURE A2 | Key steps in fabricating kombucha–chlorella bio-electronic interfaces. (1) Kombucha cellulose pellicle formation, (2) introduce microalgal culture, (3) co-culture to mature conductive mat, (4) incorporate electronic components, (5) test mat with external signals.

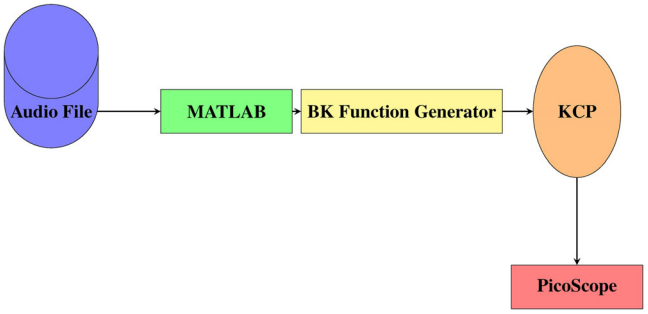

FIGURE A3 | Schematic of experimental setup and workflow.

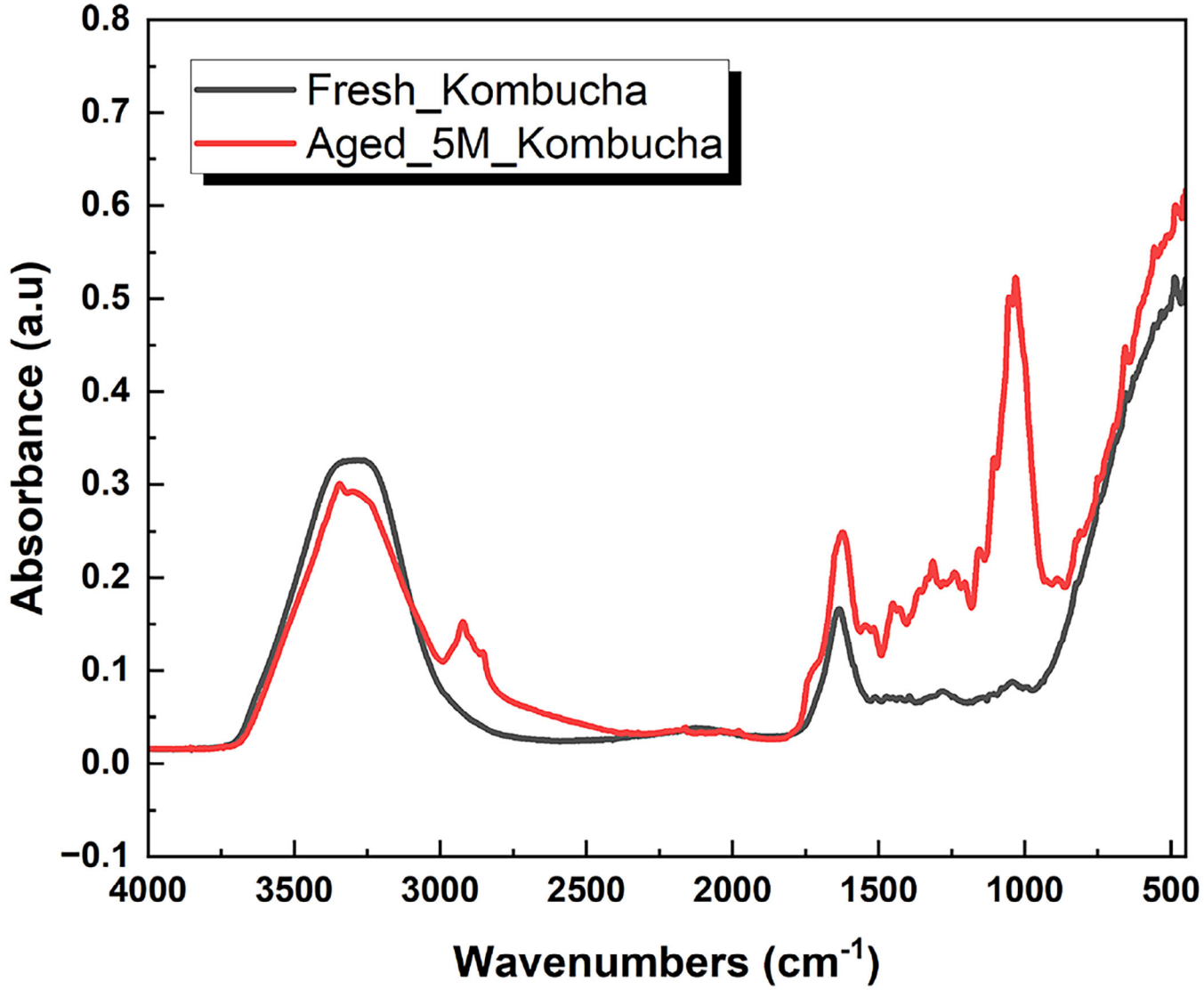

FIGURE A4 | FT-IR spectra of freshly produced and aged kombucha cellulose mats. The spectrum of a fresh kombucha cellulose mat is represented by the black line. It has distinct absorption bands at 407.96, 417.79, 448.79, and 487.24 cm^{-1}. These bands are due to the stretching and bending vibrations of the cellulose backbone. The peak observed at 3284.59 cm^{-1} is attributed to the O-H stretching vibration of hydroxyl groups inside the cellulose network. The fingerprint region (1500–500 cm^{-1}) of the cellulose mat indicates a uniform chemical composition. On the other hand, the red line illustrates the range of a kombucha cellulose mat that has been growing for 5 months. This reveals the appearance of new peaks at 1031.69 and 1314.78 cm^{-1}, which are attributed to the stretching vibrations of glycosidic linkages and the bending vibrations of cellulose, respectively. The occurrence of peaks at 1622.36 and 2922.55 cm^{-1} suggests the existence of water molecules, lignin's carbonyl groups, and aliphatic compounds. The spectrum shifts observed indicate the complex and varied chemical composition that forms in the kombucha cellulose mat as it ages.

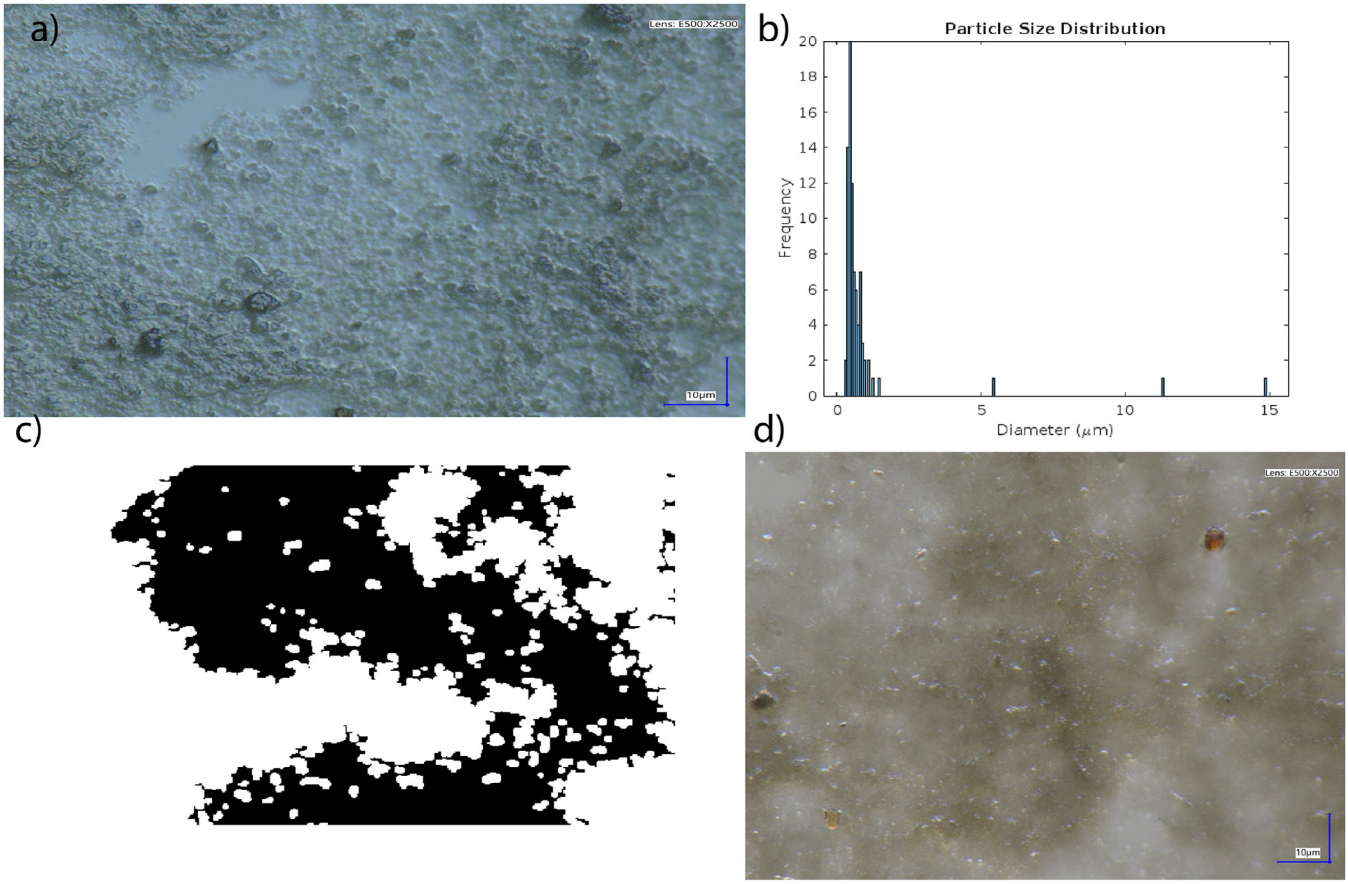

FIGURE A5 | Characterization of proteinoid microspheres. (a) Optical microscopy image acquired with a Keyence VHX–7100 optical microscope. Scale bar = 10 µm. (b) Particle size distribution of measured microsphere diameters showing a mean diameter of 0.95 µm, minimum diameter of 0.28 µm, and maximum diameter of 14.89 µm. (c) Binary threshold manipulation of the microscopy image used for calculating microsphere diameters. (d) Optical microscopy image with adjusted light orientation showing detailed morphology of proteinoid microspheres.

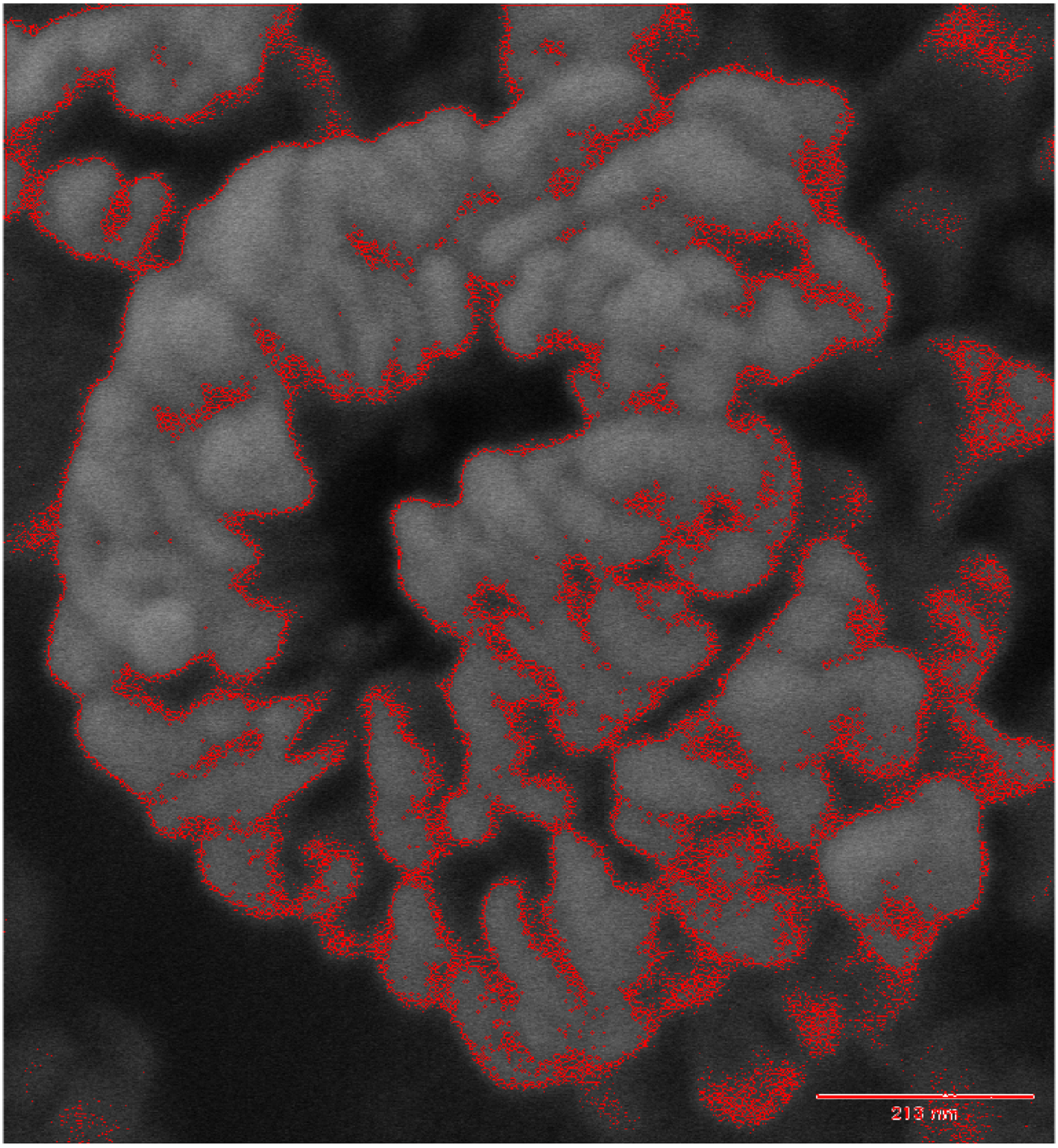

FIGURE A6 | A detailed examination of proteinoids reveals a structure consisting of interconnected nanospheres forming a complex network. A closer look reveals the intricate arrangement of proteinoid nanospheres, each measuring approximately 50 nm in diameter. These nanospheres come together to create a larger scale assembly, showcasing the remarkable organization at play. The scale bar measures 213 nm. The proteinoids were examined using an FEI Quanta 650 scanning electron microscope to analyze the nanostructural composition of these synthetic proto-brain systems. The microscopy analysis uncovers proteinoid nanoparticles that exhibit a remarkable ability to self-assemble into a complex biomimetic network with a highly spherical shape.